PHASED ARRAYS FOR METEOROLOGICAL SATELLITE

By Charles E. Profera, Jr.

June 1968

Prepared under Contract No. NAS 12-149 by:

RCA Defense Electronic Products|Missile and Surface Radar Division, Moorestown, N.J.

Electronics Research Center

NATIONAL AERONAUTICS AND SPACE ADMINISTRATION

Dr. Robert J. Mailloux
Technical Monitor
EMA
Electronics Research Center
575 Technology Square
Cambridge, Massachusetts 02139

Request for copies of this report should be referred to:

NASA Scientific and Technical Information Facility
P. O. Box 33, College Park, Maryland 20740

PHASED ARRAYS FOR METEOROLOGICAL SATELLITE

By Charles E. Profera, Jr.

June 1968

Prepared under Contract No. NAS 12-149 by:

Defense Electronic Products|Missile and Surface Radar Division,
Moorestown, N.J.

Electronics Research Center

NATIONAL AERONAUTICS AND SPACE ADMINISTRATION

CONTENTS

	Page
SUMMARY	1
INTRODUCTION	1
LINE SOURCE ARRAY	1
H-plane Line Source Element	2
Ten-element Prototype Array	4
Pattern and Impedance Evaluation	7
Other Array Measurements	9
MULTI-MODE POWER COMBINER	17
Prototype 50-way Power Combiner	25
Experimental Investigations	25
ARRAY PERFORMANCE	33
PHASE SHIFTER STUDY	46
CONCLUSIONS	49
REFERENCES	51
NEW TECHNOLOGY APPENDIX	52

ILLUSTRATIONS

Figure		Page
1	H-Plane Horn-Lens Geometry	3
2	Line Source Geometry for Pattern Computation	3
3	Computed Pattern Characteristics of H-Plane Horn Lens	5
4	Computed Patterns for H-Plane Sectoral Horn-Lens Line Source (f/d = 0.685)	5
5	Two Views of the H-Plane Horn-Lens Model	6
6	Fifty Element Array Configuration	7
7	Two Views of Ten-Element Array	8
8	Line Source H-Plane Patterns Per Element at 16.0 GHz (3 Sheets)	10
9	Expanded Scale (60-dB) Line Source Patterns at 16.0 GHz (2 Sheets)	14
10	High-Frequency H-Plane Line Source Patterns, Element 5 (2 Sheets)	15
11	VSWR Vs Frequency for Central and Edge Elements	17
12	E-Plane Patterns Per Element for H-Plane Line Source at 16.0 GHz (5 Sheets)	18
13	Inter-Element Coupling Measurements for the Ten-Element Array	23
14	Path-Length Difference Among Elements of the Ten-Element Array	24
15	Relative Gain Per Element for the 10-Element Array at 16.0 GHz	24
16	Configuration of N-Way Power Combiner With Tapered Distribution	26

ILLUSTRATIONS (Continued)

Figure		Page
17	Prototype 50-Way Power Combiner	26
18	E-Plane Multi-Mode Horn Lens Patterns (3 sheets)	27
19	E-Plane 50-Way Power Combiner Patterns (3 sheets)	30
20	Uncorrected Amplitude and Phase Characteristics of the 50-Way Power Combiner at 16.0 GHz	33
21	Five-Section Phase Shifter	33
22	Phase Shift and VSWR As A Function of Screw Turns for 5-Section Phase Shifter	34
23	Phase-Corrected E-Plane 50-Way Power Combiner Patterns (5 Sheets)	35
24	Power Combiner VSWR Vs Frequency With All Ports Terminated in Matched Loads	39
25	Lens-Divider Section of Power Combiner VSWR Vs Frequency	40
26	Ten-Element Array With 50-Way Power Combiner	40
27	H-Plane Patterns for Power-Combiner/Array Configuration (3 Sheets)	41
28	Spherical Coordinate System	44
29	Projected Array Beam Efficiency	47
30	Ferrite-Loaded Waveguide Cross Section	47
31	Toroid Shape	48

PHASED ARRAYS FOR METEROLOGICAL SATELLITE

by Charles E. Profera, Jr.

SUMMARY

An H-plane sectoral horn-lens line source has been developed for use in a Ku-band phased array. A prototype ten-element array of these line source elements was constructed and tested. Inter-element spacing is consistent with a maximum scan requirement of ±60°. Element patterns recorded over the 15.2 to 16.8 GHz frequency band exhibit extremely low sidelobes with no maximum sidelobes exceeding -32 dB. Line source patterns and relative gain measurements give no indication of undesirable effects due to element location within the array.

Multi-mode techniques were employed in the design of a fifty-way power combiner for use with an array of fifty line source elements. Combiner radiation patterns agree very well with those of the E-plane sectoral multi-mode horn-lens antenna which is an integral part of the combiner. Maximum sidelobe levels of approximately -30 dB are obtained at 16.0 GHz. Sidelobe performance deteriorates toward the 15.2 to 16.8 GHz frequency band edges.

Beam efficiency* is computed using measured line source and combiner pattern data. Beam efficiency exceeds 90 per cent over the 15.2 to 16.8 GHz band, 93 per cent over the 15.6 to 16.8 GHz band, and 96 per cent at 16.0 GHz.

A study was also conducted to determine the phase shifter requirements and problems inherent in electronically scanning the array beam to ±60°.

INTRODUCTION

This report discusses the analysis and evaluation of the critical components of a highly efficient Ku-band phased array antenna with single-plane electronic scan capability.

Performance characteristics of a prototype, low-sidelobe ten-element line-source array and 50-way power combiner are presented.

Studies of a five-bit ferrite phase shifter for electronic scan application are discussed.

LINE SOURCE ARRAY

Line source element studies discussed in the first interim report (Ref. 1) were concerned with use of a reduced-width E-plane multi-mode sectoral horn as a radiating

*Fraction of the total available antenna power received within the angular region defined by the main beam of the antenna pattern.

element. The bandwidth of such an element was at best on the order of 5% due to the proximity of the horn width to the cut-off dimension for a ±30° scan capability. Because of the scan and bandwidth limitations of the reduced-width multi-mode horn, consideration was given to a new line source element design. At an early meeting with Dr. R. D. Kodis and Dr. R. Mailloux of the National Aeronautics and Space Administration, Electronics Research Center, a polarization change for the line source element was suggested. By agreement among all interested persons, no particular sense of linear polarization was considered preferable for the intended application of this antenna. Therefore, the development work herein reported was conducted without regard to a specific polarization.

H-Plane Line Source Element

The desired low-sidelobe, high beam efficiency characteristics required of the Ku-band array can be realized using the simple wide flare angle, dominant mode, H-plane sectoral horn with dielectric lens (Ref. 2) shown in Figure 1 as a line source element. Extreme bandwidths are available from this element because it is a single-mode device which employs a lens with an index of refraction that is essentially invariant with frequency.

A brief analysis was conducted to determine the radiation characteristics of an H-plane sectoral horn-lens line source radiator with a half-power beamwidth of approximately 3°.

The H-plane radiation pattern of the H-plane sectoral horn-lens antenna is given by equation (1) for the line source geometry of Figure 2.

$$E(\theta) = \left[2 \sum_{y=m}^{d/2} T(y) \cos\frac{\pi y}{d} \cos\left(\frac{2\pi y}{\lambda} \sin\theta\right) \right] + T(0) \qquad (1)$$

T(y) is the lens "taper" factor and is given by

$$T(y) = L \left[\frac{1}{(L + nx)\,(L + x(n+1)} \right]^{1/2}$$

where

$$x = \frac{L}{n+1} \left\{ \left[1 + \frac{y2}{L^2} \frac{(n+1)}{(n-1)} \right]^{1/2} - 1 \right\}$$

L = distance from focal point to lens surface along axis of horn

n = index of refraction

λ = wavelength

m = sampling increment

Equation (1) was programmed for the IBM 1620 and patterns were computed for the horn geometry of Figure 2 with d = 17.5 inches. The ratio of lens focal length to horn line source dimension (f/d) was varied to determine the optimum value. A polystyrene lens with $\epsilon_r = 2.55$ was assumed. The index of refraction, n, for the H-plane sectoral horn is approximately $\sqrt{\epsilon_r}$ at all frequencies of interest.

Computed half-power beamwidth and maximum sidelobe levels at 16.0 GHz are plotted in Figure 3 as a function of f/d. Computed patterns for an H-plane sectoral horn-lens with f/d = 0.685 are plotted in Figure 4 for operating frequencies of 15.2, 16.0 and 16.8 GHz. It is observed in the preceding data that low sidelobe capabilities are inherent in the wide flare angle H-plane sectoral horn-lens antenna over a wide frequency band.

The H-plane sectoral horn-lens line source element has a further advantage over E-plane types when used in an array configuration. The propagation constant of the dominant mode in the H-plane horn, like that of standard rectangular waveguide, is dependent only on the transverse dimension orthogonal to the electric field vector and is independent of the horn height "b" in Figure 1. This implies that, in an array geometry, the horn height can be sufficiently reduced to provide for single-plane inter-element spacings of one-half wavelength or less, thereby preventing formation of unwanted grating lobes for any forward hemisphere scan requirement.

In order to demonstrate acceptable line source performance, before proceeding with fabrication of a prototype array, a single H-plane horn-lens with d = 17.6 inches and f/d = 0.743 was fabricated and evaluated experimentally. This design was chosen as a compromise of sidelobe level and horn focal length, f. Photographs of this model are shown in Figure 5. Measured antenna patterns exhibit the desirable low sidelobe radiation characteristics.

Ten-element Prototype Array

A Ku-band array of H-plane sectoral horn-lens elements are designed to give an approximate 3° half-power beamwidth and provide a scan capability of at least ±60° avoiding grating lobe formation. The horn f/d ratio is 0.743 with a line source dimension of 17.6 inches. The array is designed so that the inter-element spacing is one half wavelength at 16.8 GHz corresponding to the high frequency edge of a 10% frequency band centered at 16.0 GHz. This design prevents formation of grating lobes

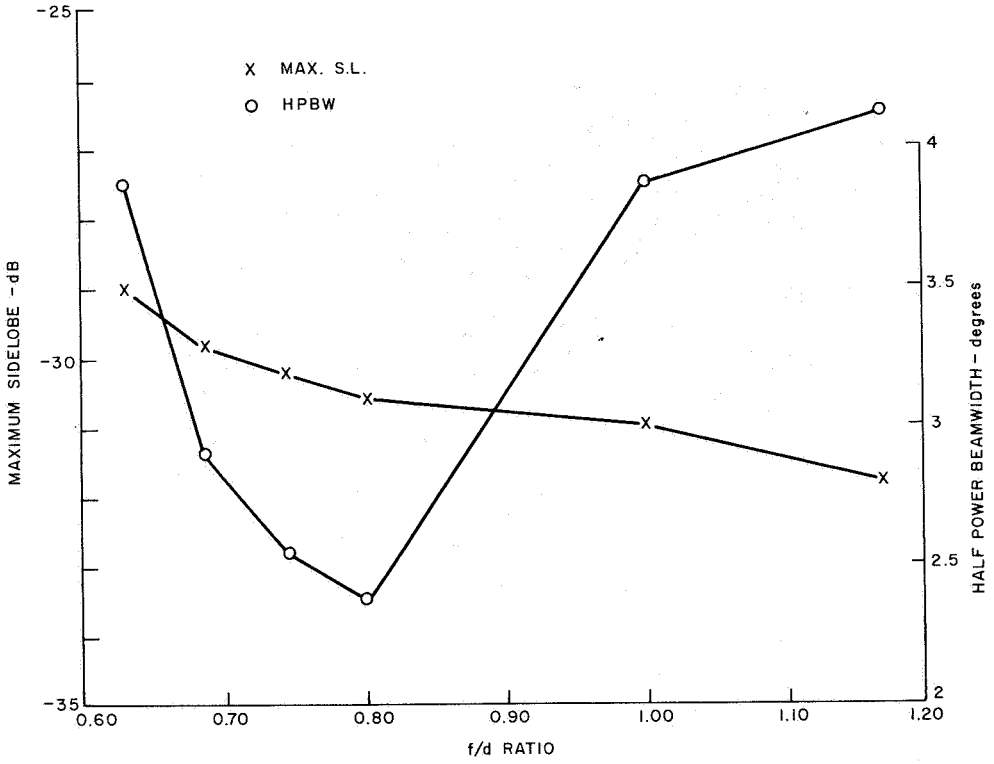

Figure 3. Computed Pattern Characteristics of H-Plane Horn Lens

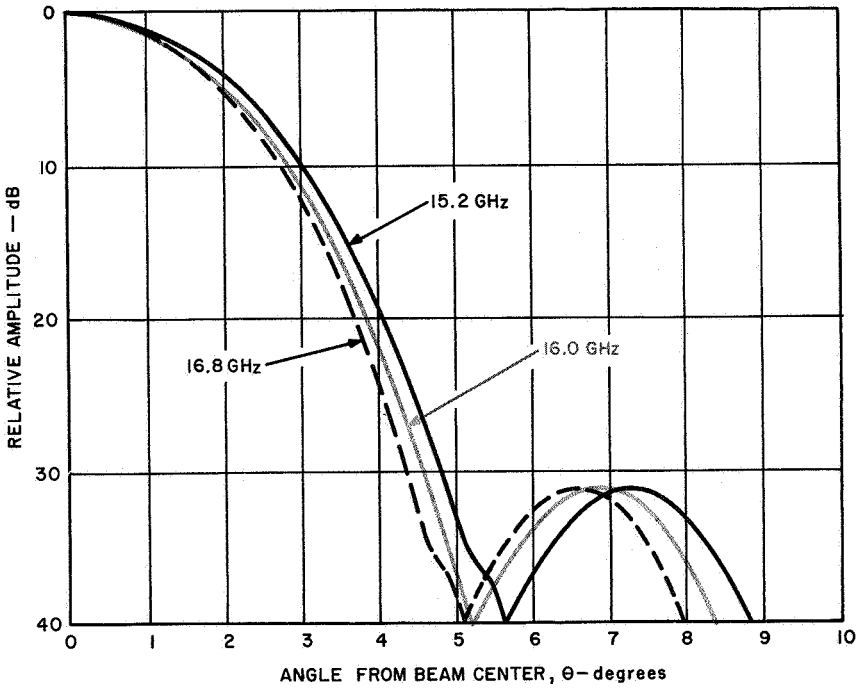

Figure 4. Computed Patterns of H-Plane Sectoral Horn-Lens Line Source for f/d = 0.685

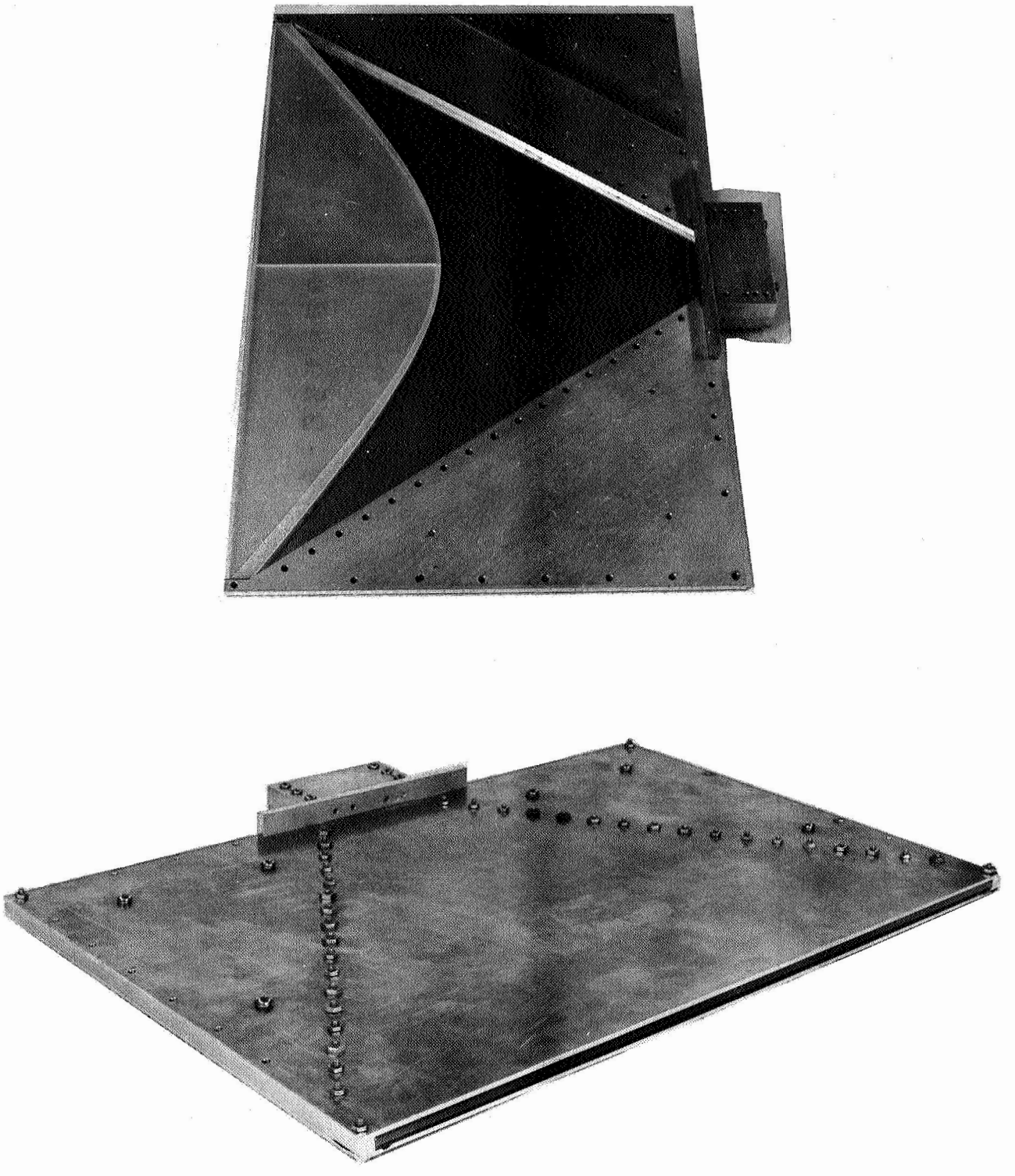

Figure 5. Two Views of the H-Plane Horn-Lens Model

within a ±90° scan angle for the 15.2 to 16.8 GHz frequency band. The array configuration for a 3° half-power beamwidth requires approximately 50 H-plane horn-lens line source elements, as shown in Figure 6.

The ten-element array of H-plane sectoral horn-lens line source elements was fabricated. The array is constructed of aluminum and retains the basic dimensions shown in Figure 6. Commercial grade polystyrene is used for lens fabrication. Quarter-wave matching transformer sections (Ref. 3) are provided on the input and output surfaces of each lens to provide the necessary impedance match.

Photographs of the complete prototype array are shown in Figure 7. Quarter-wave waveguide transformers are used at the 0.622 x 0.259-inch waveguide inputs to the array to provide transition to standard WR 62 waveguide.

Pattern and Impedance Evaluation

A test program was initiated to determine the pattern and impedance characteristics of the individual line source elements in an array environment. Pattern and impedance characteristics of the central elements in the ten-element array are indicative of the majority of elements in a full 50-element array. Edge elements in the ten-element array exhibit pattern and impedance characteristics like those of the outermost elements of the full 50-element array.

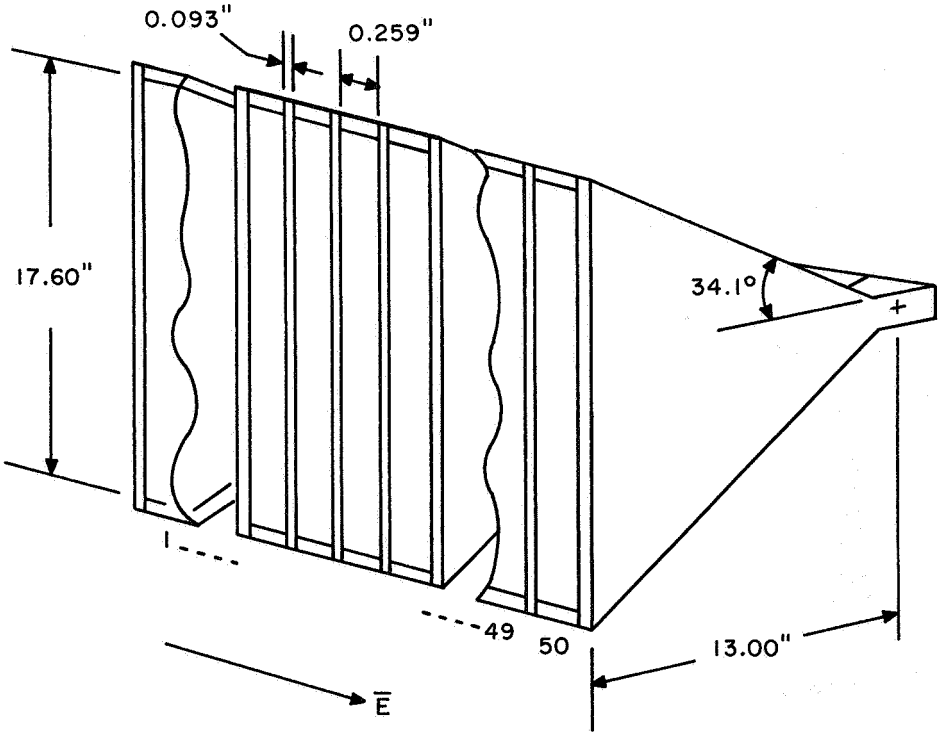

Figure 6. Array Configuration

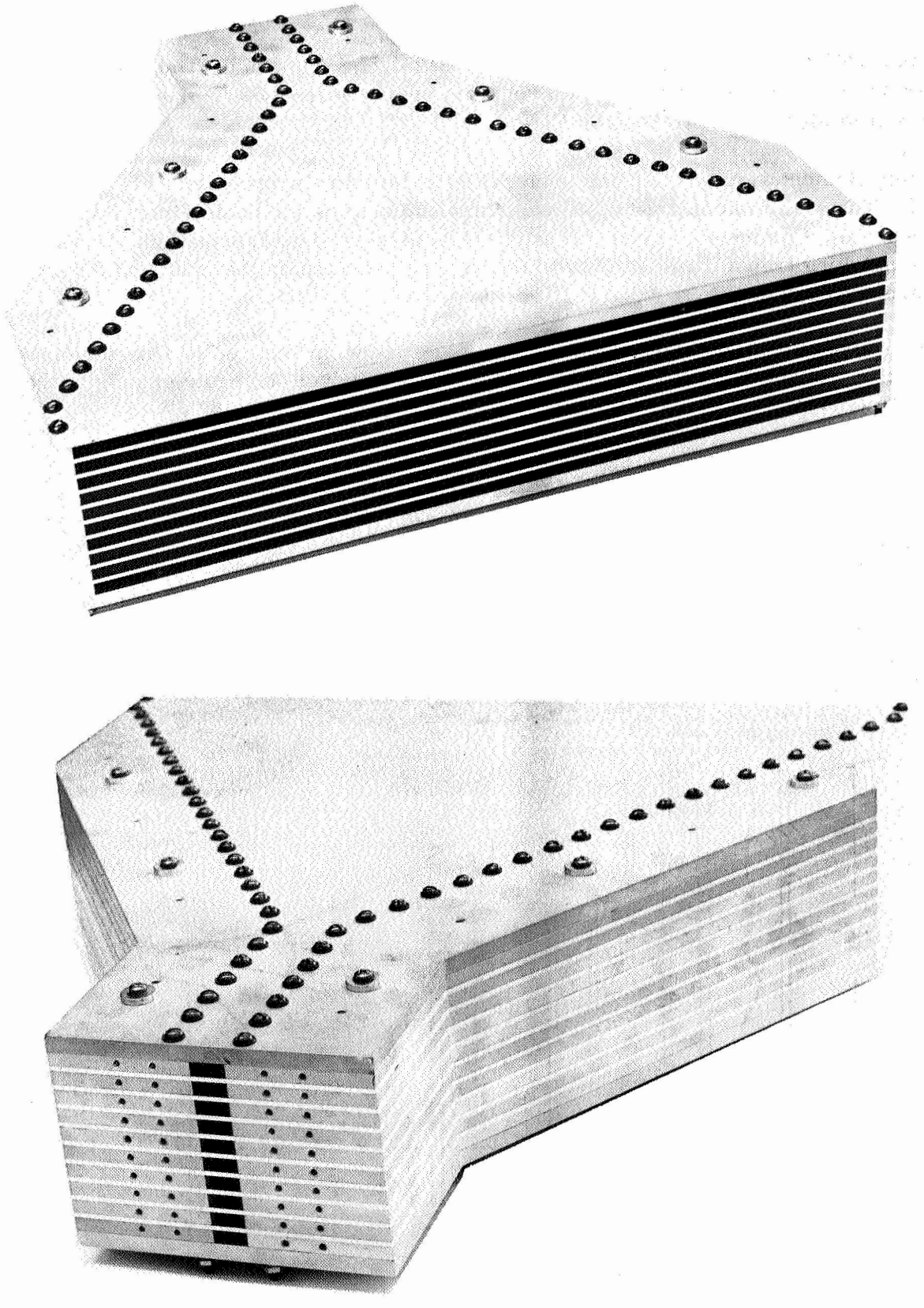

Figure 7. Two Views of Ten-Element Array

The H-plane radiation patterns of elements 1 through 10 at 16.0 GHz are shown in Figure 8. Table I summarizes the maximum sidelobe level and beamwidth data obtained per element over the 15.2 to 16.8 GHz frequency band. In all cases shown, no sidelobe exceeds -32 dB implying that the projected beam efficiency of an array with principal-plane patterns equivalent to that of a single H-plane line source will be extremely high (in excess of 97.5% for most cases). Pattern measurements were repeated on a 60-dB scale to obtain additional sidelobe information. Several such patterns are shown in Figure 9. The low sidelobe characteristics obtained are very critically dependent on the impedance match at the horn-lens and lens-free space interface. However, a broad-band match is easily obtained through use of lens surface matching quarter-wave transformers and it was found that excellent low-sidelobe pattern characteristics are available over a frequency band in excess of 10%. Line source pattern data was obtained over the 15 to 21 GHz band with essentially the same results as previously shown. Examples of the high frequency patterns are shown in Figure 10.

Impedance data was obtained for the individual elements. VSWR vs frequency plots for a central and edge element are shown in Figure 11. Both the pattern data of Figure 8 and Table I and the impedance data of Figure 11 show that the H-plane pattern and impedance of the line source are relatively unaffected by element location within the array and are not subject to edge effects.

E-plane patterns of the individual elements of the ten-element array are shown in Figure 12. A skewing of the E-plane pattern maximum is observed for those elements closest to the edge. This skewing effect is reduced at elements proceeding toward the array center. For a complete 50-element array, the edge effects influence only the E-plane radiation characteristics of the outermost elements (two or three in from the edge) which elements are only very lightly illuminated due to aperture distribution tapering which is provided in the array plane. It is expected that this edge effect will not severely influence performance of the complete array.

Other Array Measurements

Inter-element coupling levels were determined for the ten-element array. Data was obtained by exciting a specific element and measuring the signal coupled to the remaining nine elements. Measured data is plotted in Figure 13 for several single element excitations.

A theoretical analysis of the inter-element coupling in an array of parallel plate waveguides has been performed by Lee (Ref. 4). The experimental determination of inter-element coupling levels for the ten-element array agrees extremely well with that predicted for the array of parallel plate waveguides in Ref. 4.

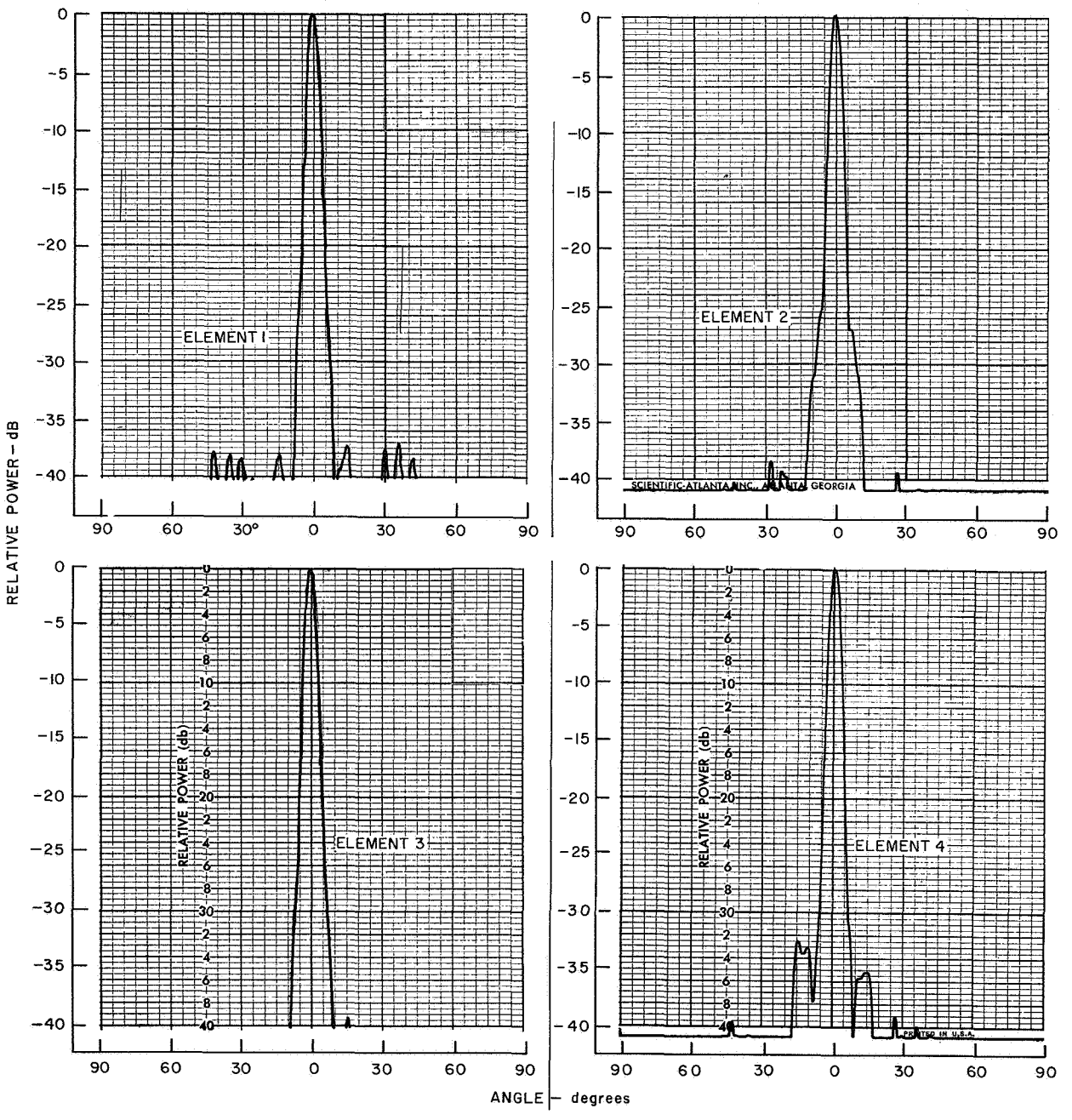

Figure 8. Line Source H-Plane Patterns Per Element at 16.0 GHz (Sheet 1 of 3)

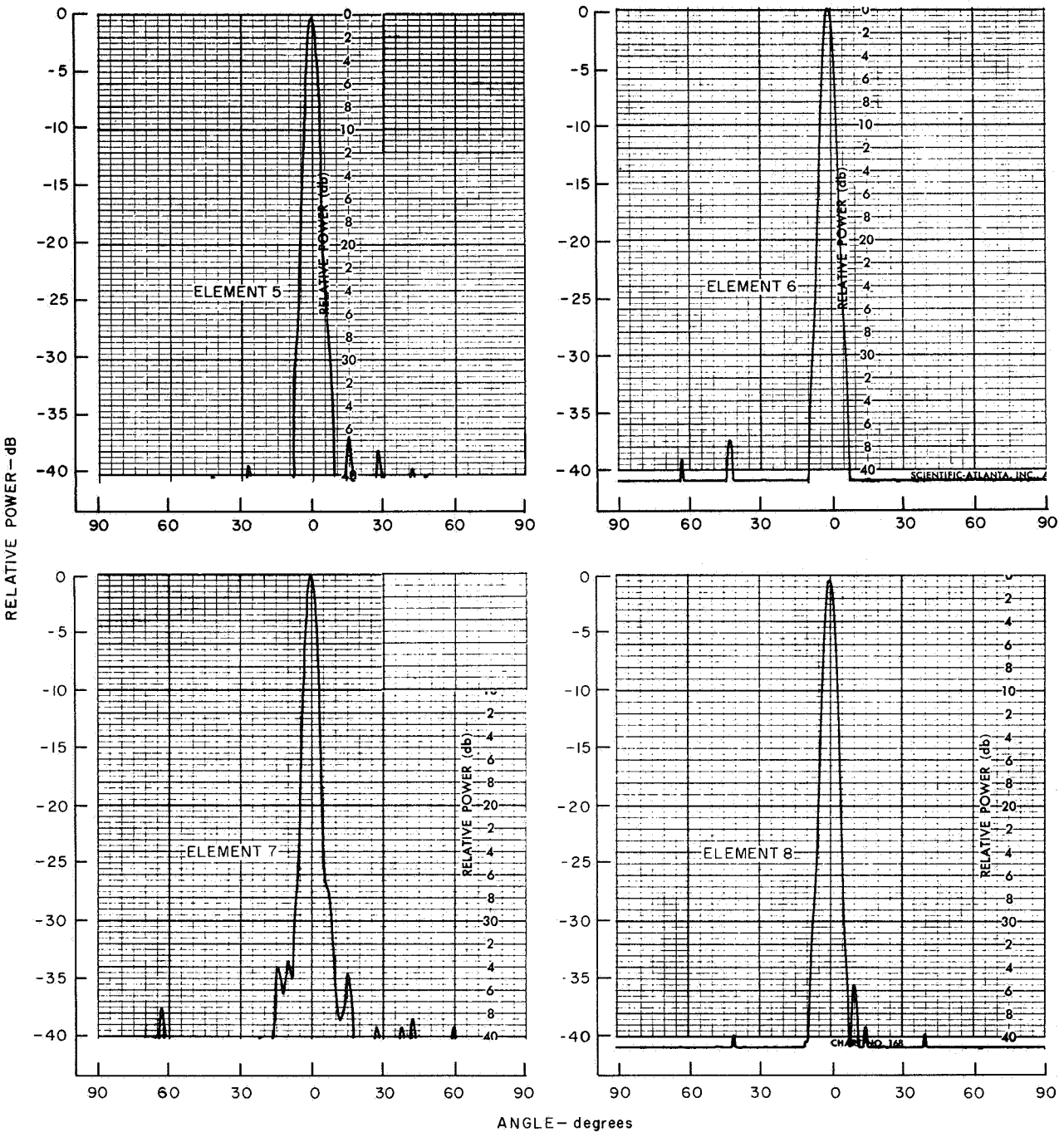

Figure 8. Line Source H-Plane Patterns Per Element at 16.0 GHz (Sheet 2 of 3)

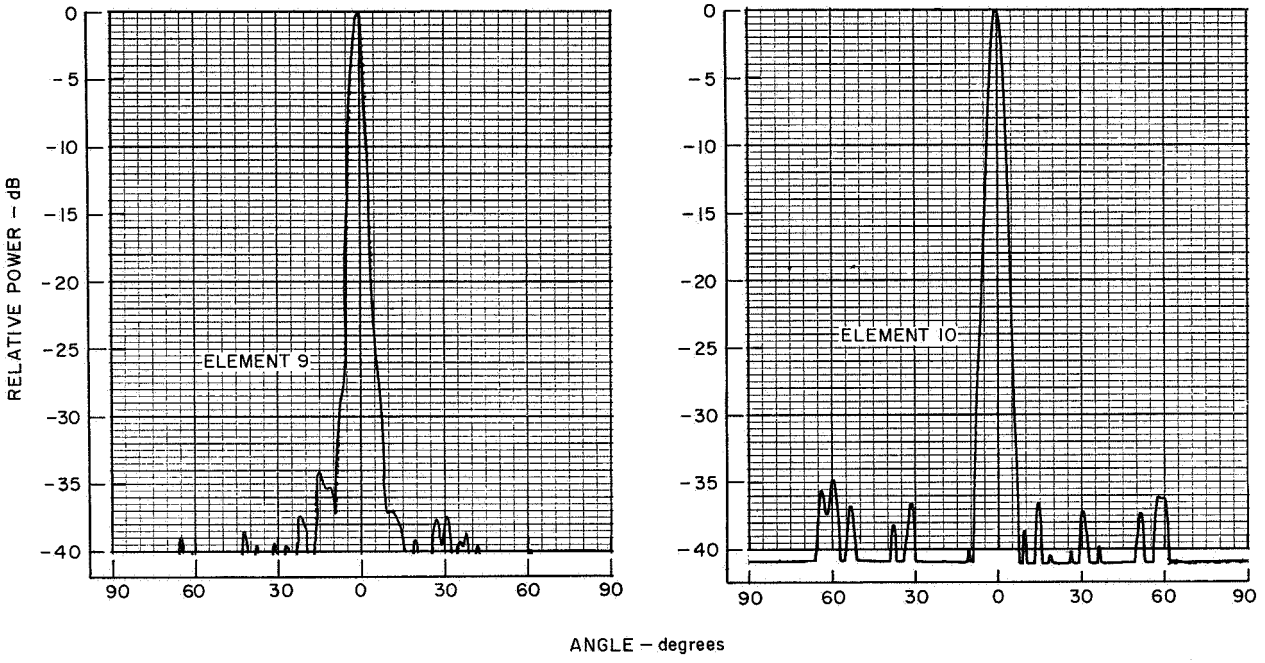

Figure 8. Line Source H-Plane Patterns Per Element at 16.0 GHz (Sheet 3 of 3)

TABLE I. MAXIMUM SIDELOBE LEVELS PER ELEMENT FOR TEN-ELEMENT ARRAY

Element Number	Maximum Sidelobe (dB)				
	Frequency (GHz)				
	15.2	15.6	16.0	16.4	16.8
1	-34.5	-40	-37	-37.5	-36
2	-32	-34	-38	-36.5	-36.5
3	-37	-36	-39	-37	-34.5
4	-33.5	-36.5	-32.5	-34	-32.5
5	-35	-34.5	-36.5	-35	-34
6	-37	-36.5	-37.5	-39	-33.5
7	-36	-39	-33.5	-34	-36.5
8	-35.5	-34	-35.5	-35	-32.5
9	-34	-34	-34	-33.5	-37
10	-32	-34	-35	-36	-36
	Average Half-power Beamwidth (degrees)				
	3.9	3.8	3.7	3.5	3.4

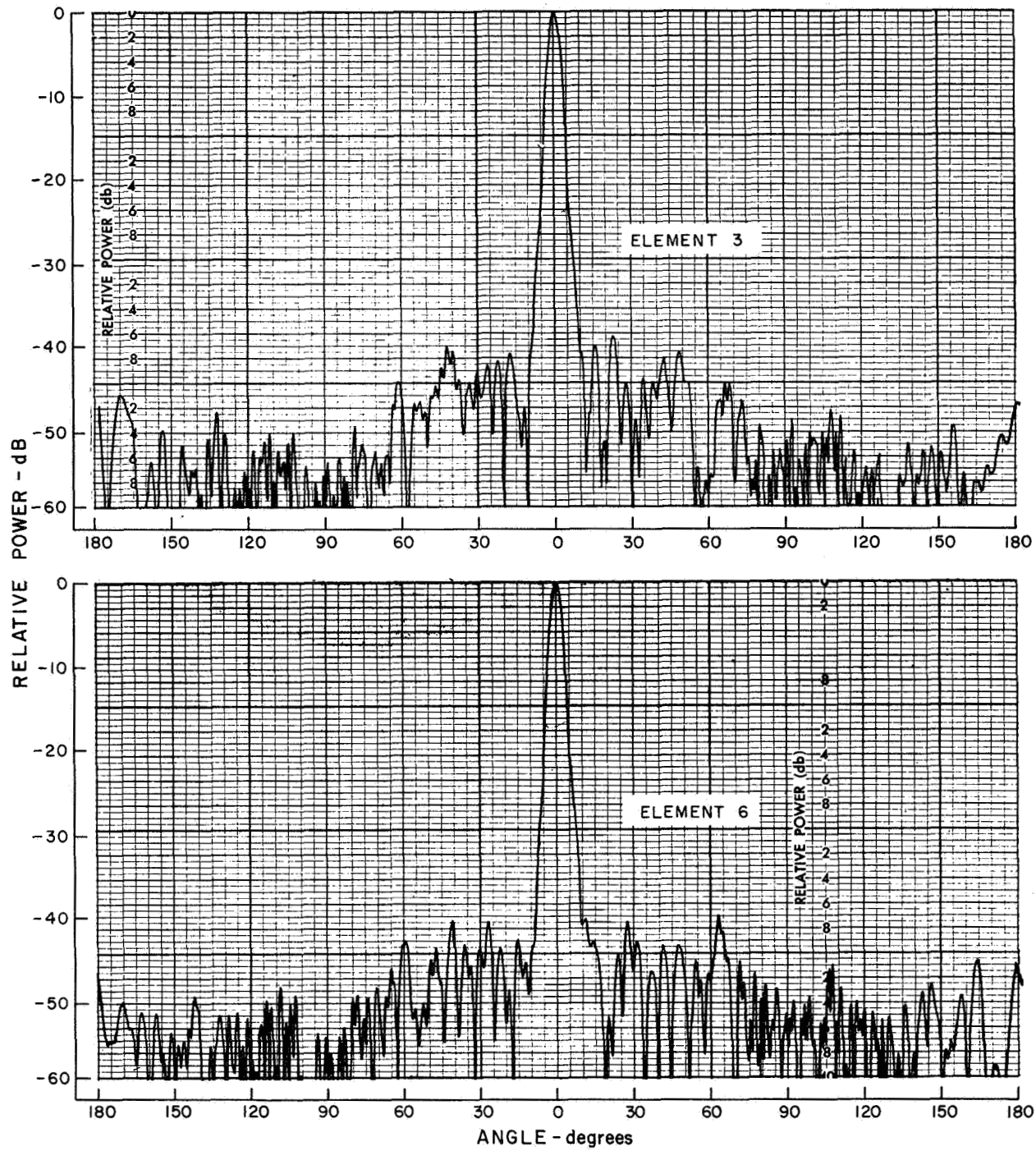

Figure 9. Expanded Scale (60-dB) Line Source Patterns at 16.0 GHz (Sheet 1 of 2)

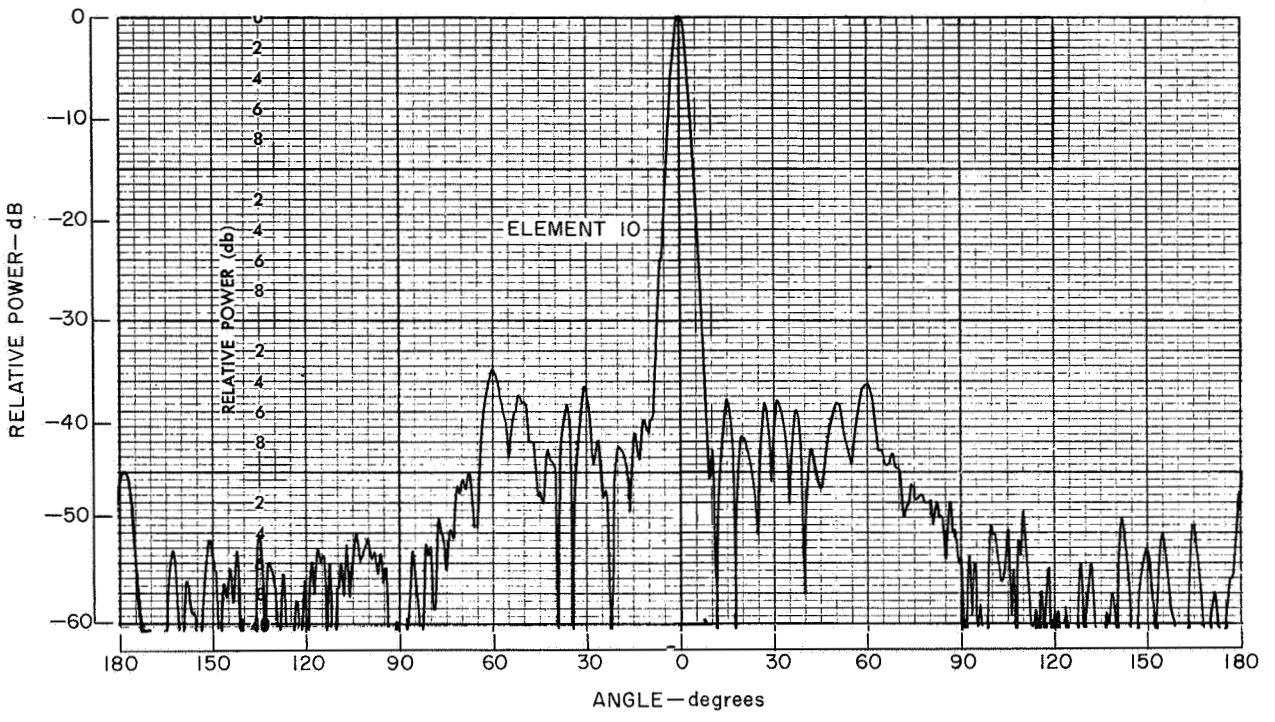

Figure 9. Expanded Scale (60-dB) Line Source Pattern at 16.0 GHz (Sheet 2 of 2)

Relative path-length differences were measured through the individual horns comprising the 10-element array. This data was obtained to determine the extent of phase equality of the individual horns of the array and to evaluate the array fabrication technique. Path length differences vs. element number are plotted in Figure 14. Path lengths through the horn are essentially equal for elements symmetrically disposed about the center. Edge effects are noted in the deviation of the phase difference of the outer element pairs from that of the centrally located elements.

Gain measurements were made on the individual line source elements comprising the ten-element array. Relative gain difference between elements was determined. Relative gain difference at 16.0 GHz is plotted versus element location in Figure 15. The data does not indicate a substantial gain change between edge and center elements. Absolute element gain was determined by the comparison method using a commercial calibrated standard gain horn. The measured gain of the centrally-located element number five is 19.4 dB.

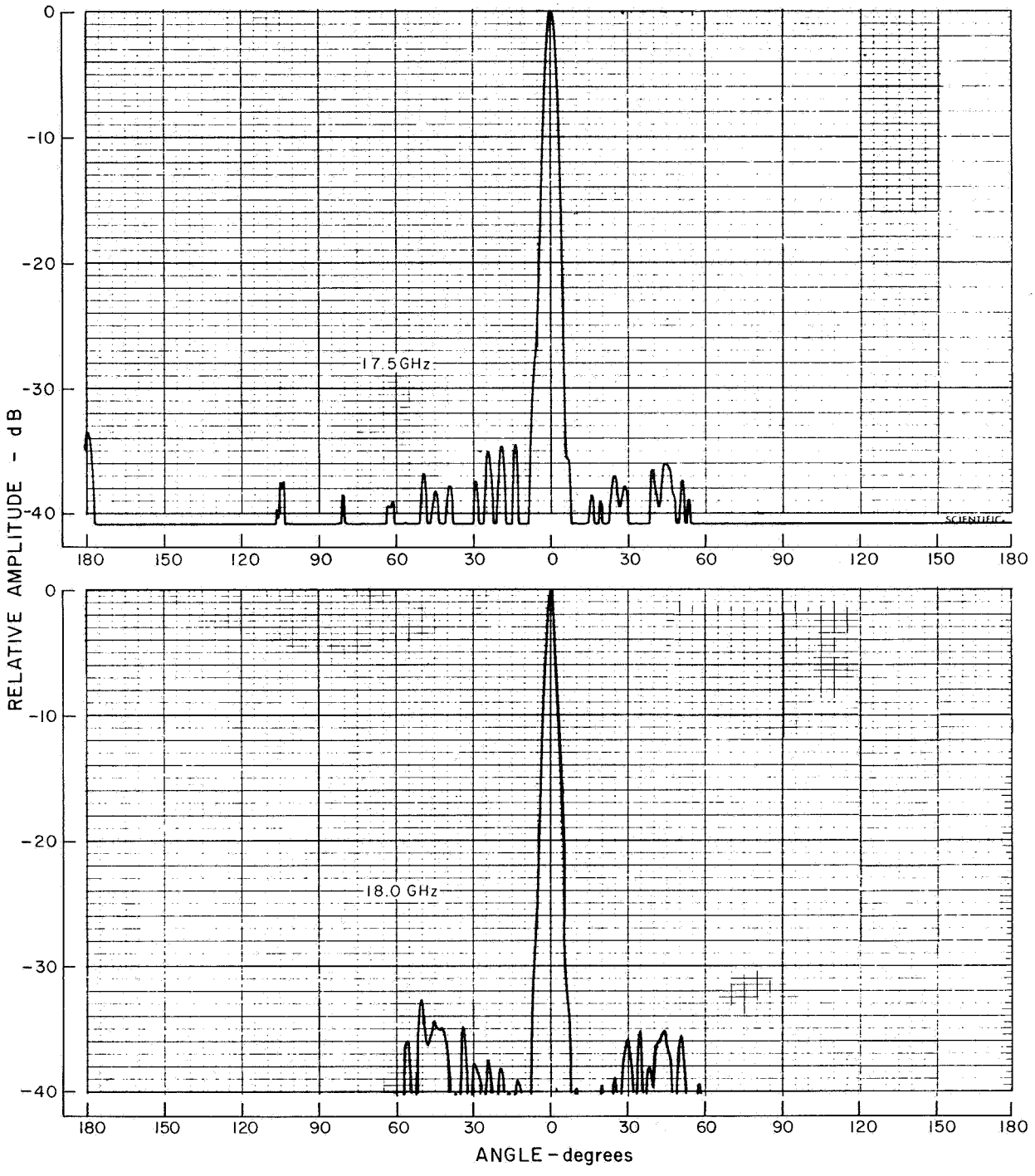

Figure 10. High-Frequency H-Plane Line Source Patterns, Element 5 (Sheet 1 of 2)

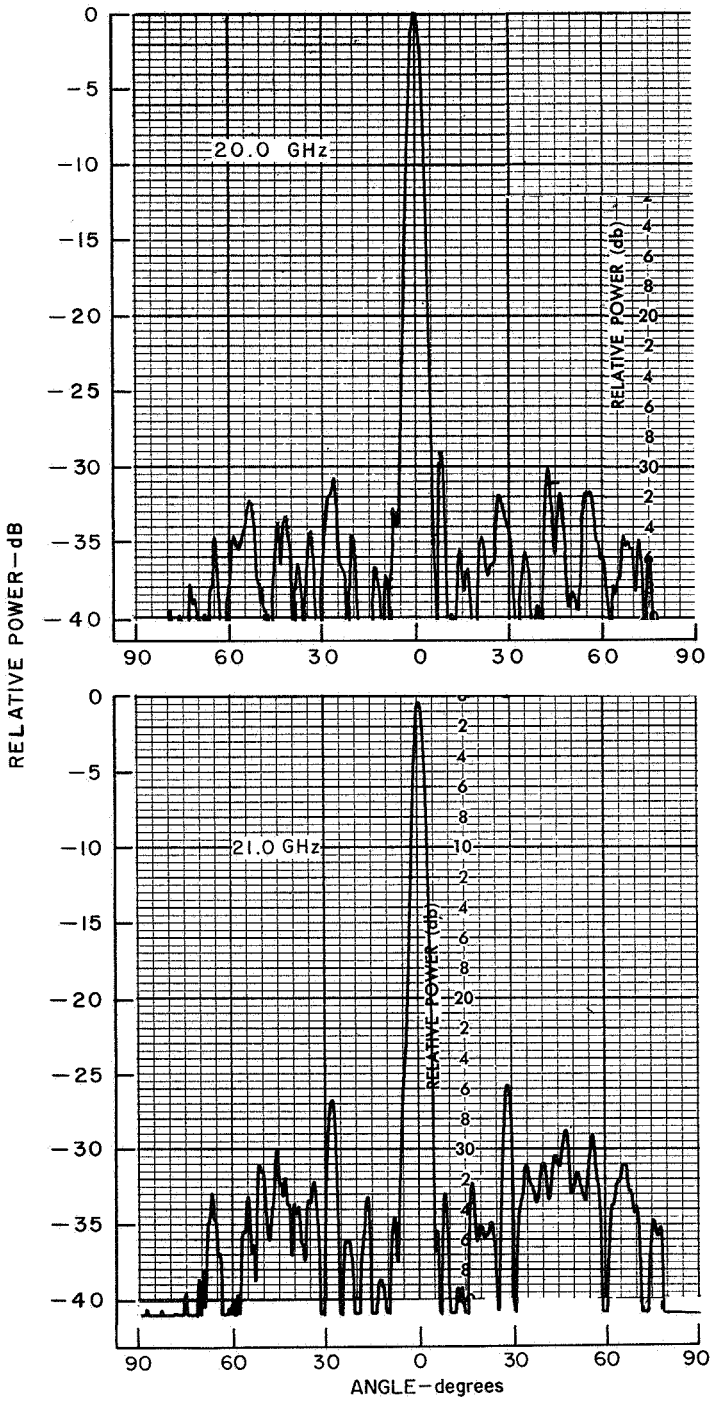

Figure 10. High-Frequency H-Plane Line Source Patterns, Element 5 (Sheet 2 of 2)

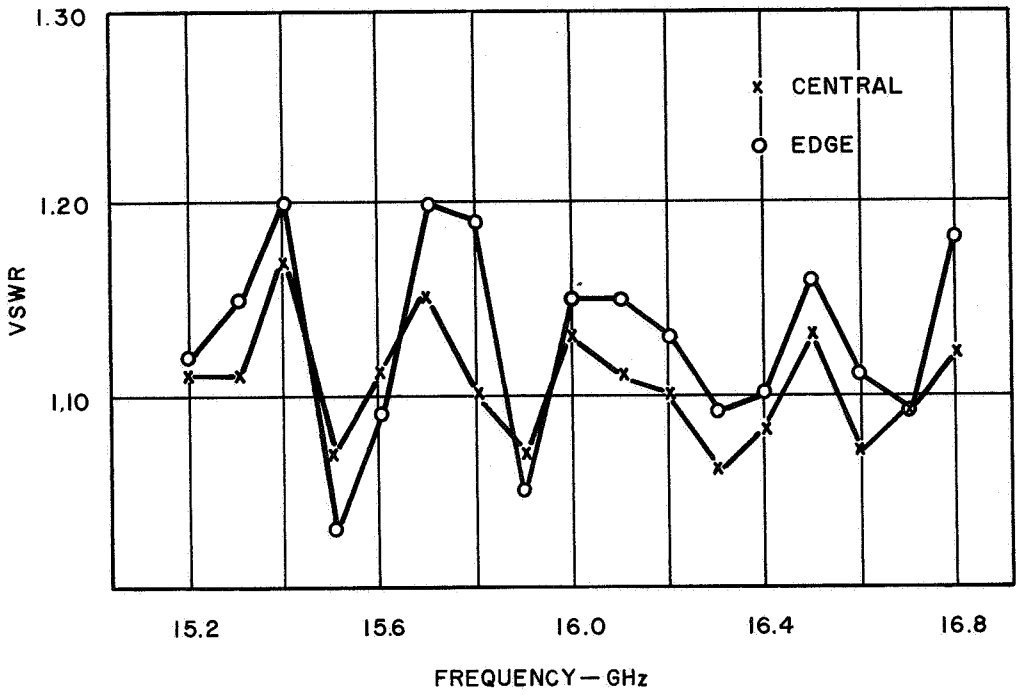

Figure 11. VSWR vs Frequency for Central and Edge Elements

MULTI-MODE POWER COMBINER

The power combiner required for the full array must have performance characteristics similar to the basic line source element. That is, it must be capable of producing an array plane pattern characterized by low sidelobes and subject to high beam efficiency. This is accomplished by providing specific tapered aperture distributions across the combiner output where the combiner is being thought of as a transmitting N-way power divider. In addition to the radiation requirements, the power combiner must be a low-loss device capable of providing an N-way divided output.

All of the above requirements are satisfied using an optical power combiner consisting of an E-plane multi-mode sectoral horn-lens waveguide* with an N-way divided output. The power combiner is shown conceptually in Figure 16.

*The previously stated agreement (page 2) of polarization change for the line source element and ten-element array necessarily dictates a change from the term H-plane beamformer appearing in the work statement of this contract. The power combiner employed here is an E-plane beamformer since this type device is more readily adaptable to the new array configuration.

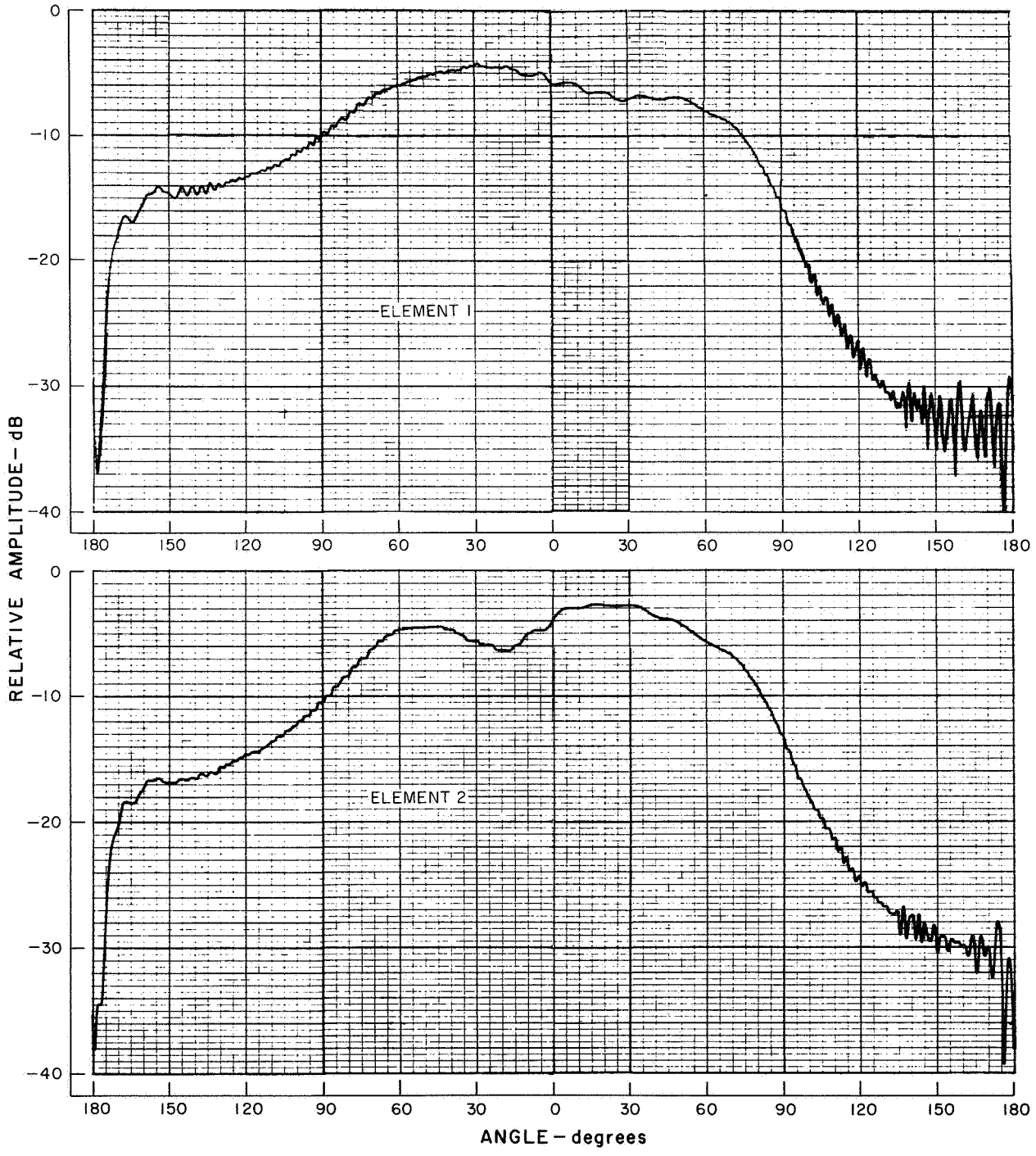

Figure 12. E-Plane Patterns Per Element for H-Plane Line Source at 16.0 GHz (Sheet 1 of 5)

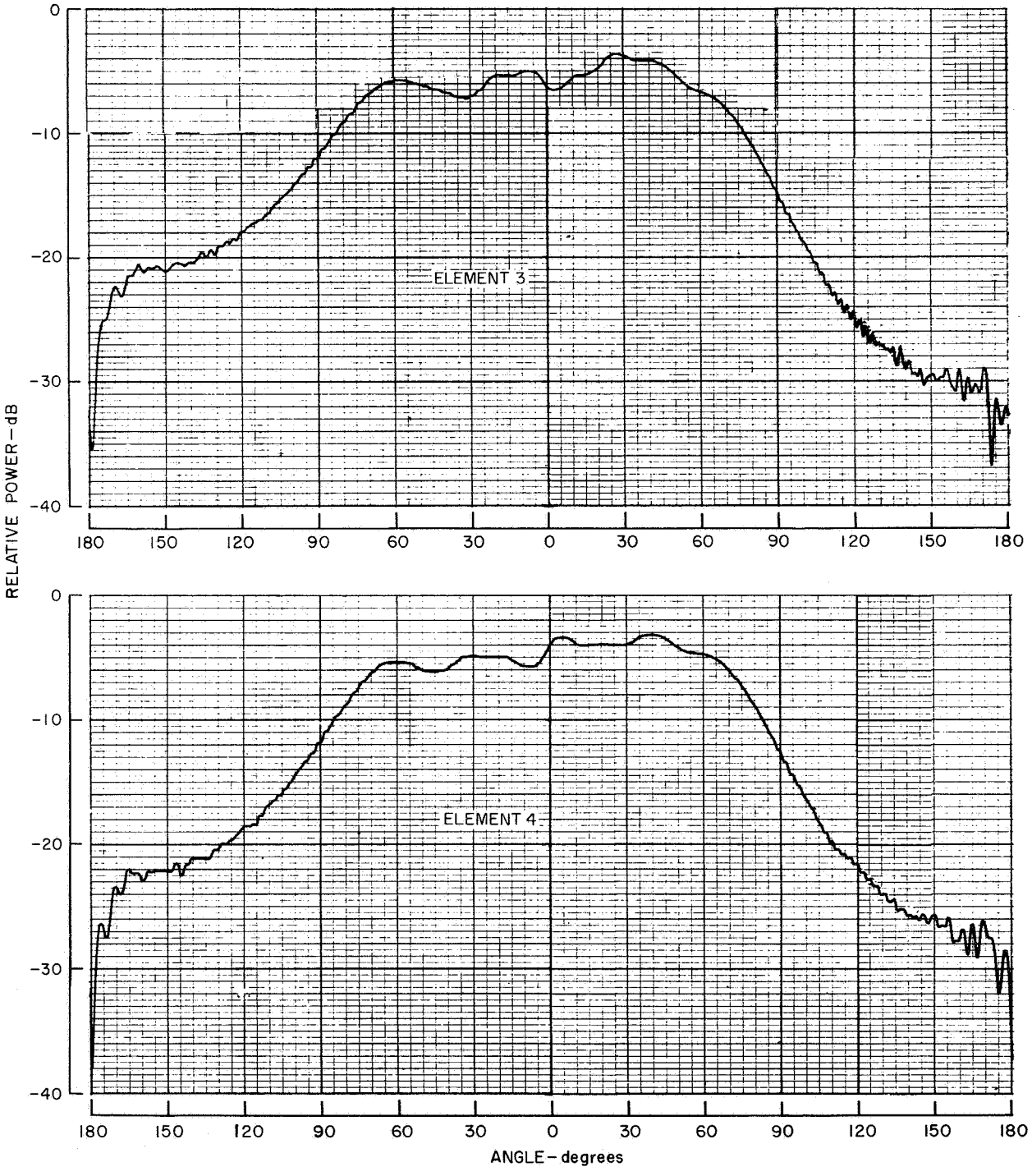

Figure 12. E-Plane Patterns Per Element for H-Plane Line Source at 16.0 GHz (Sheet 2 of 5)

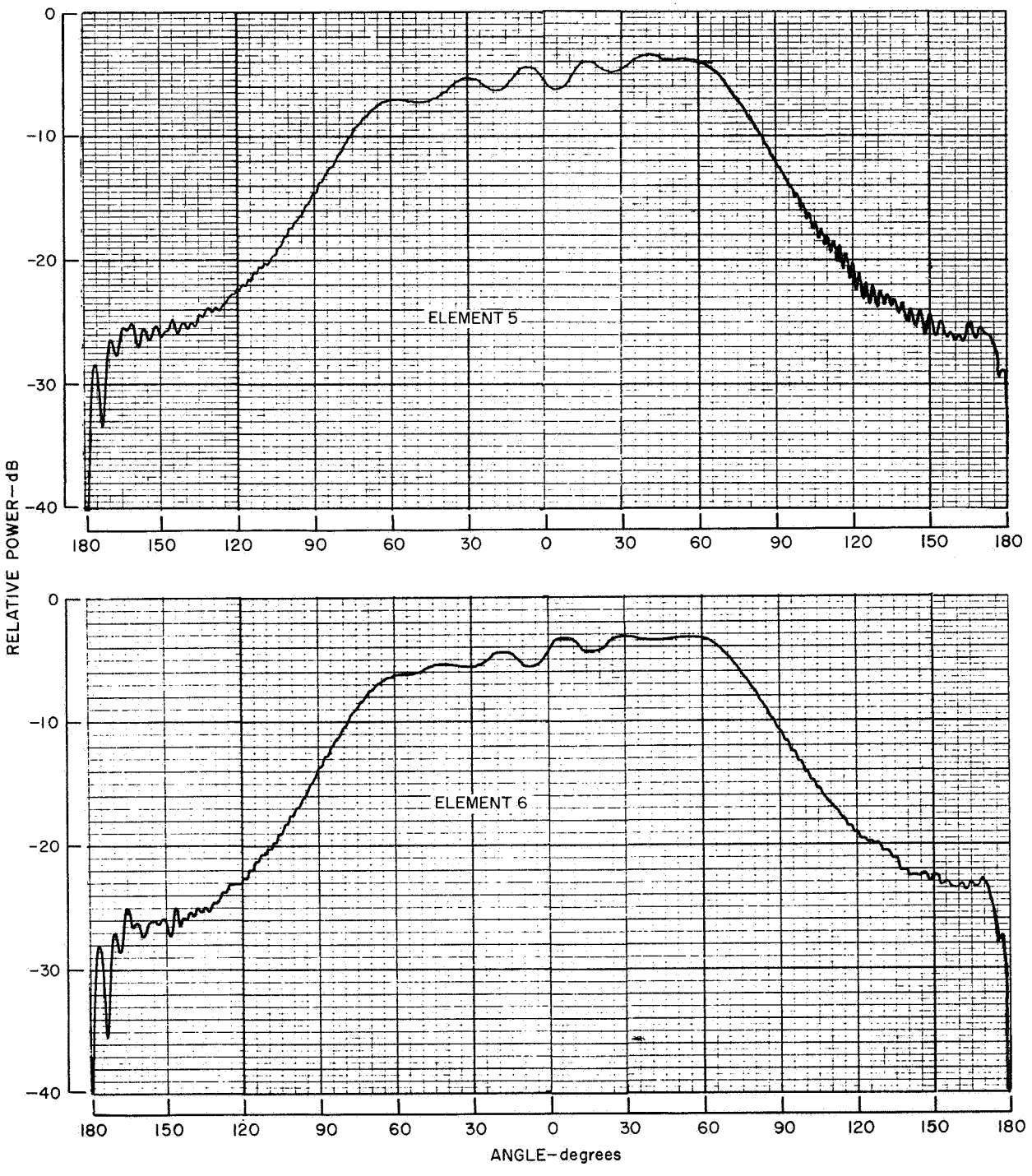

Figure 12. E-Plane Patterns Per Element for H-Plane Line Source at 16.0 GHz (Sheet 3 of 5)

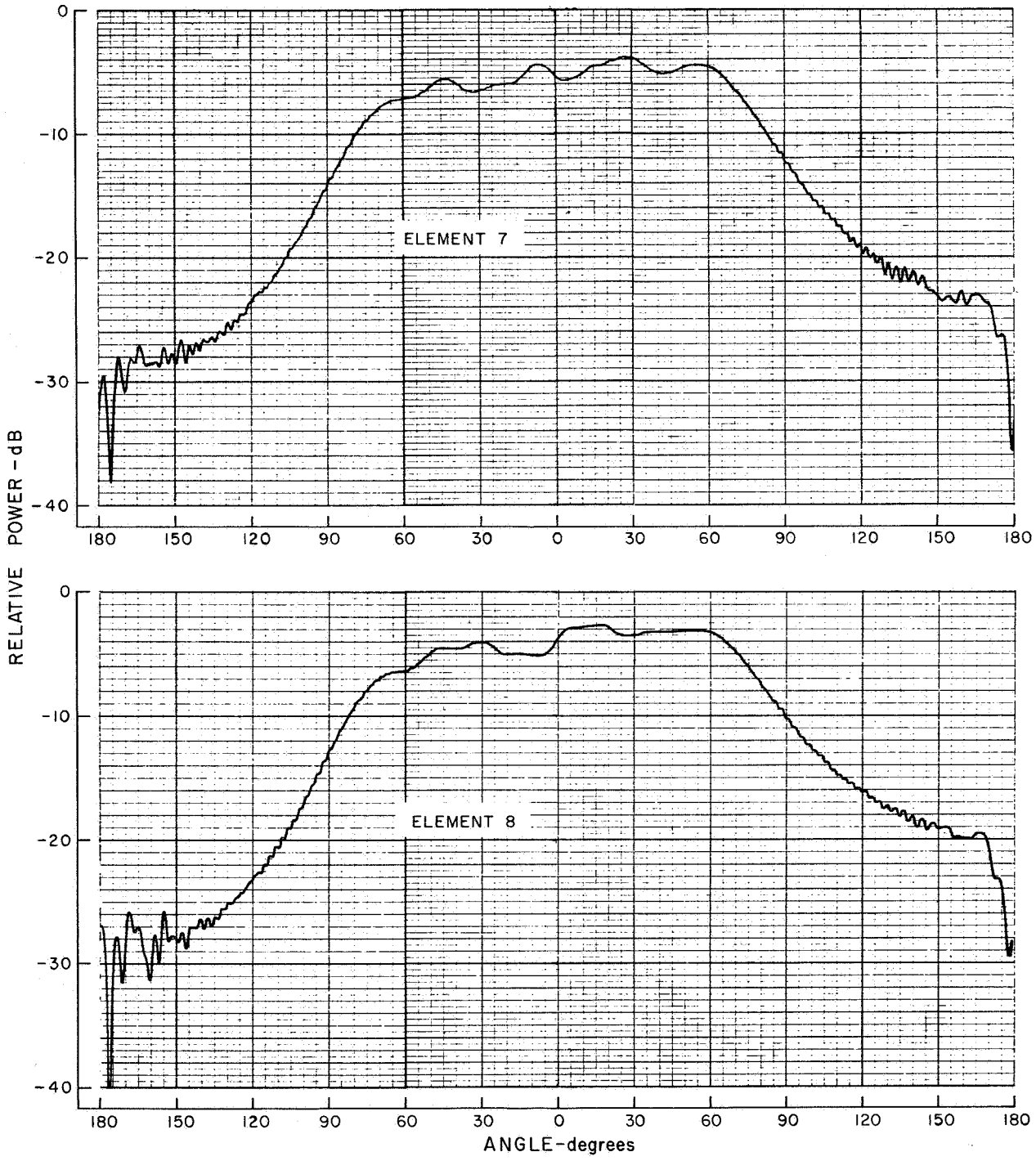

Figure 12. E-Plane Patterns Per Element for H-Plane Line Source at 16.0 GHz (Sheet 4 of 5)

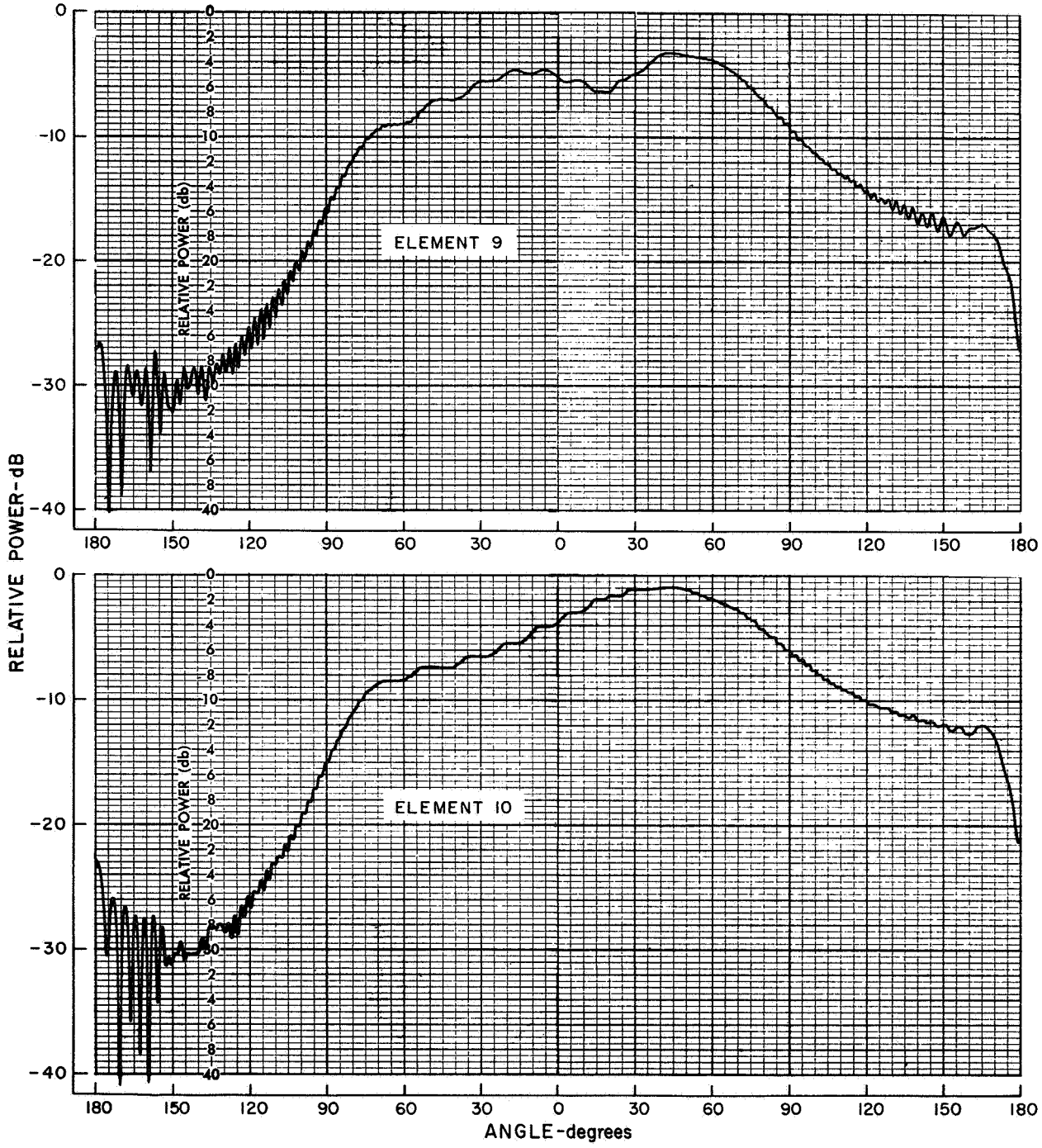

Figure 12. E-Plane Patterns Per Element for H-Plane Line Source at 16.0 GHz (Sheet 5 of 5)

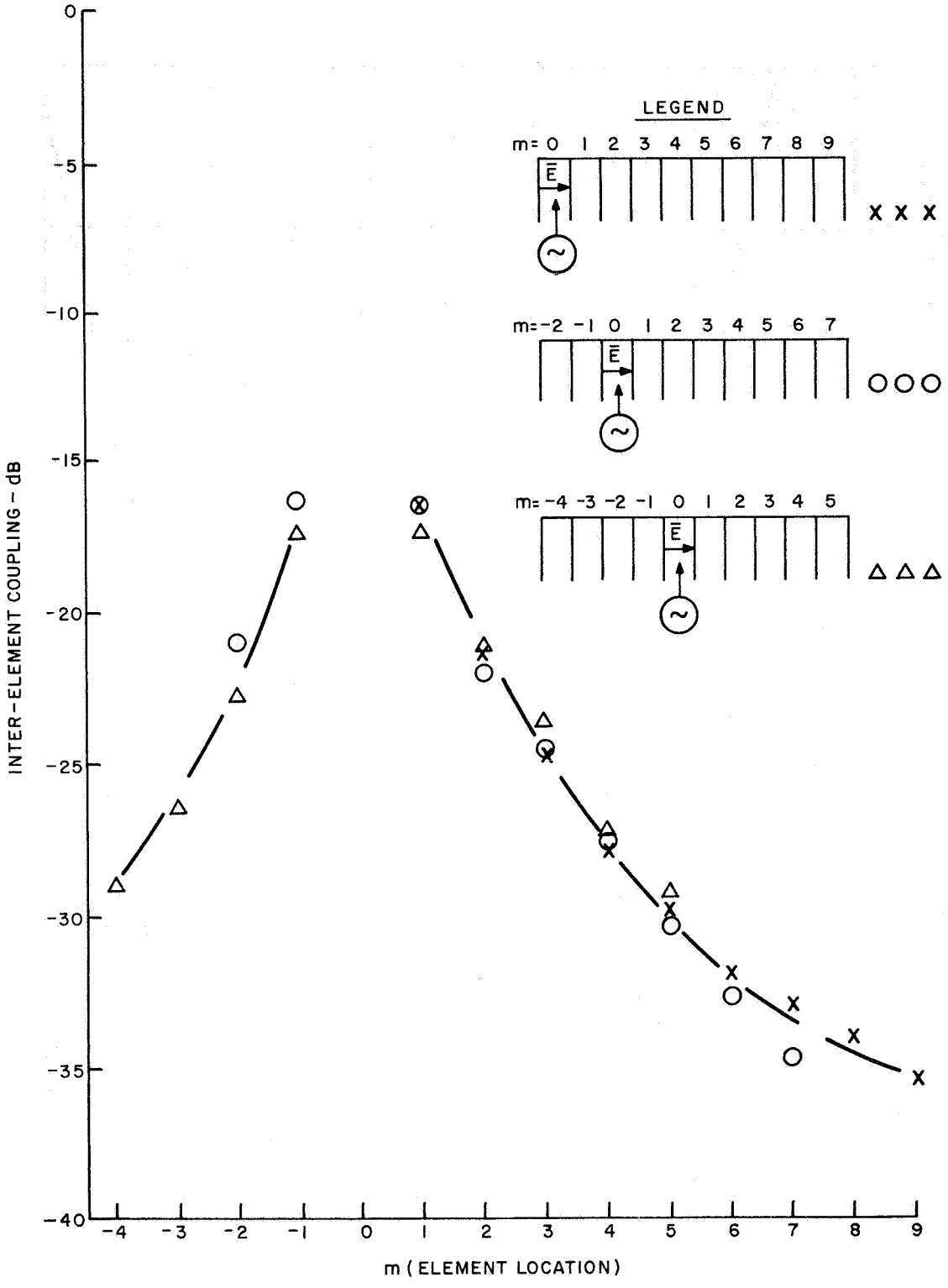

Figure 13. Inter-Element Coupling Measurements for Ten-Element Array (m=o is the Excited Element)

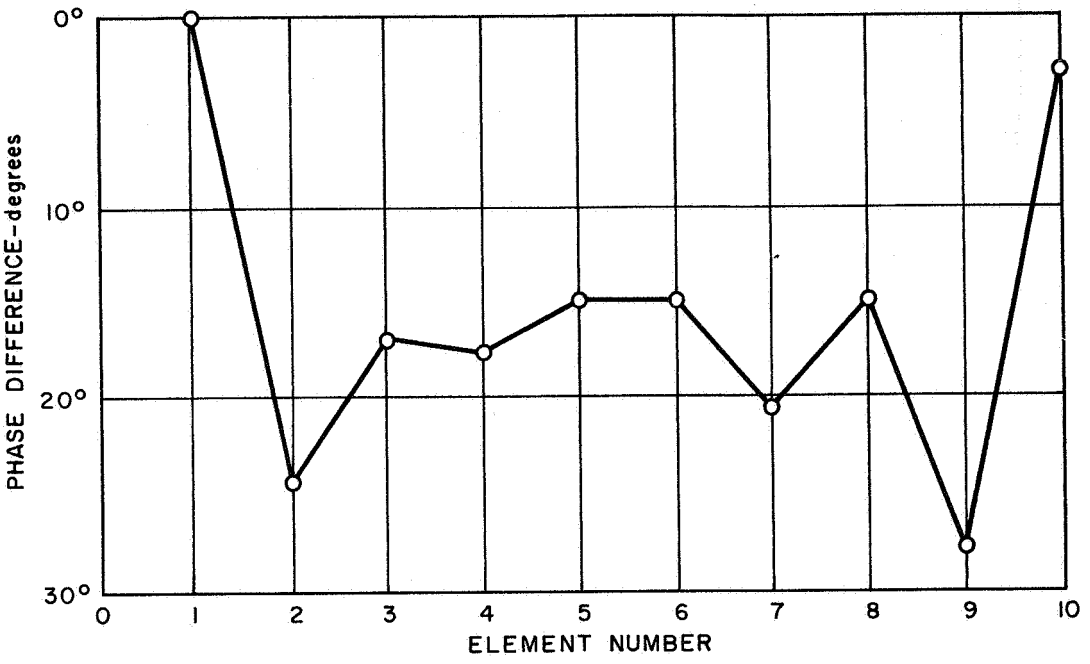

Figure 14. Path-Length Difference Among Elements of the Ten-Element Array

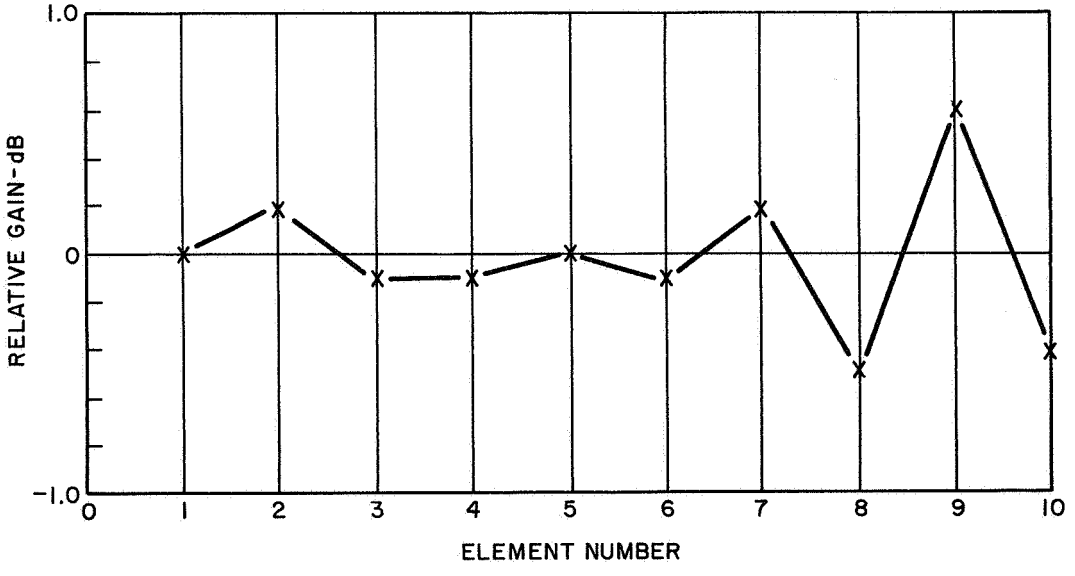

Figure 15. Relative (to Element No. 1) Gain Per Element for the Ten-Element Array at 16.0 GHz

Tapered aperture distributions are readily provided by generation of the H_{12} sectoral horn mode in combination with the dominant H_{10} mode at the horn throat (Ref. 1). Selection of the proper H_{12} to H_{10} mode amplitude ratio will provide tapered distributions resulting in satisfactory radiation patterns. The N-way divided output is provided by terminating the horn with a linear E-plane array of rectangular waveguide elements. Dividing walls employed are thin and normal to the electric field vector of the incident wave over most of this region so that their presence does not appreciably change the field configuration at the horn output nor give rise to unwanted mode generation.

Bandwidth is achieved by making the horn width sufficiently larger than the H_{10} mode cutoff dimension for the lowest operating frequency while at the same time restricting this dimension to prevent generation of unwanted higher order modes.

An advantage of the E-plane multimode sectoral horn power combiner in the array configuration is the natural interface of combiner output to array input. No additional waveguide components such as twists or impedance transformers are necessary if the combiner output waveguide dimensions and the array element input waveguide dimensions are designed to be equal.

Prototype 50-Way Power Combiner

A prototype 50-way power combiner was designed using a previously developed multimode horn geometry. The multimode horn geometry employed is the split multi-mode horn described in Ref. 1. This horn provides for generation of the H_{10} mode with an antiphased pair of H_{11} modes (equivalent to the H_{12} mode) in adjacent half horns for aperture distribution control. The divider section is a linear E-plane array of fifty rectangular 0.622 x 0.259-inch waveguides with 0.093-inch thick E-plane walls. The divider element dimension equals the input waveguide dimension of the individual line source horns. Quarter wave transformer sections are employed as an integral part of the divider to provide an impedance match to the multimode horn-lens output. A photograph of the multimode power combiner is shown in Figure 17.

Experimental Investigations

The radiation characteristics of the fifty-way combiner should be almost equal to those of the multimode horn-lens model if the divider section is well made and introduces no phase or amplitude irregularities of its own. In order to determine the radiation characteristics of the power combiner and evaluate its performance, radiation patterns were measured of both the multimode horn-lens section and a full combiner radiating as a linear waveguide array. Radiation patterns of the multimode horn-lens section over the 15.2 to 16.8 GHz frequency band as shown in Figure 18. Patterns of the complete 50-way power combiner are shown in Figure 19. Some increase in the average sidelobe level is noted in the power combiner patterns. This increase is due primarily to electrical path length differences between individual elements of the divider.

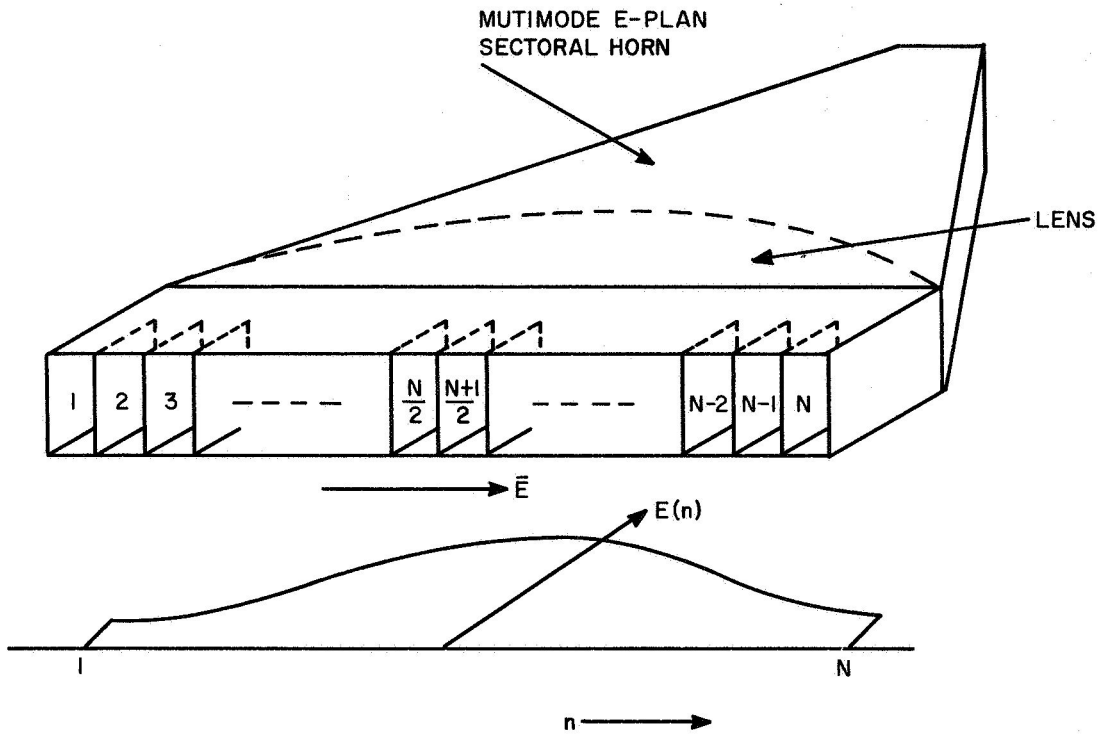

Figure 16. N-Way Power Combiner With Tapered Distribution

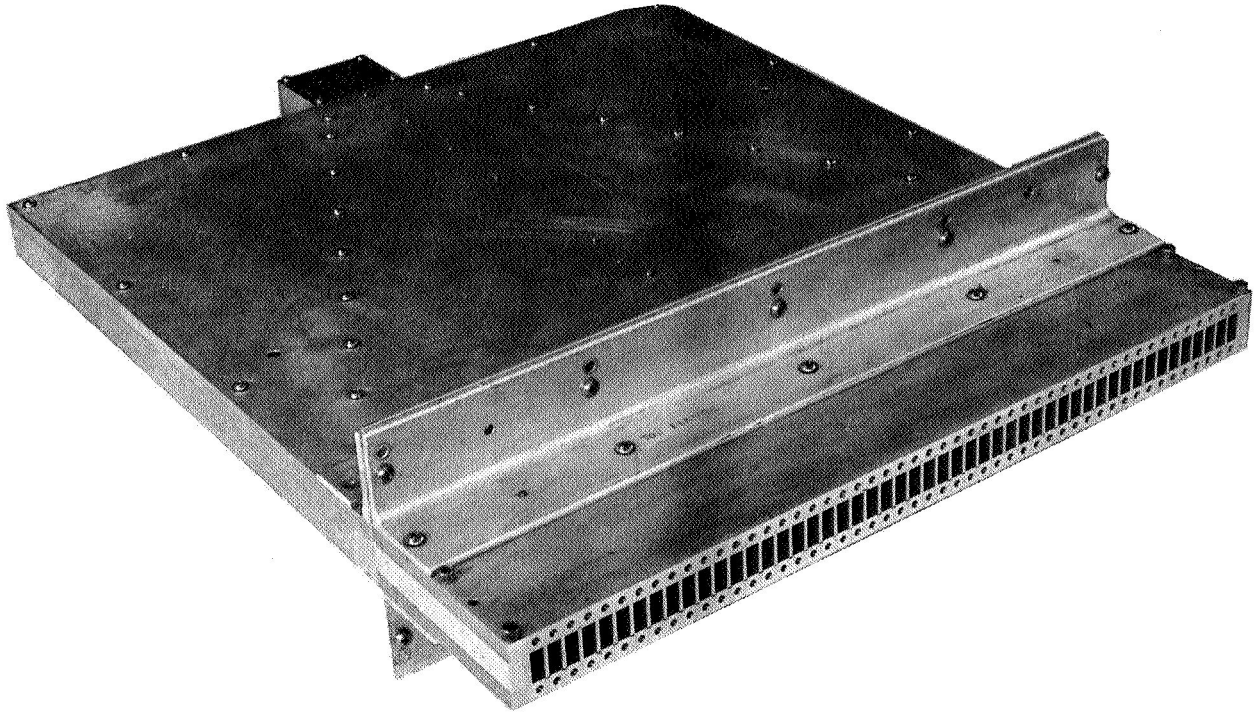

Figure 17. Prototype 50-Way Power Combiner

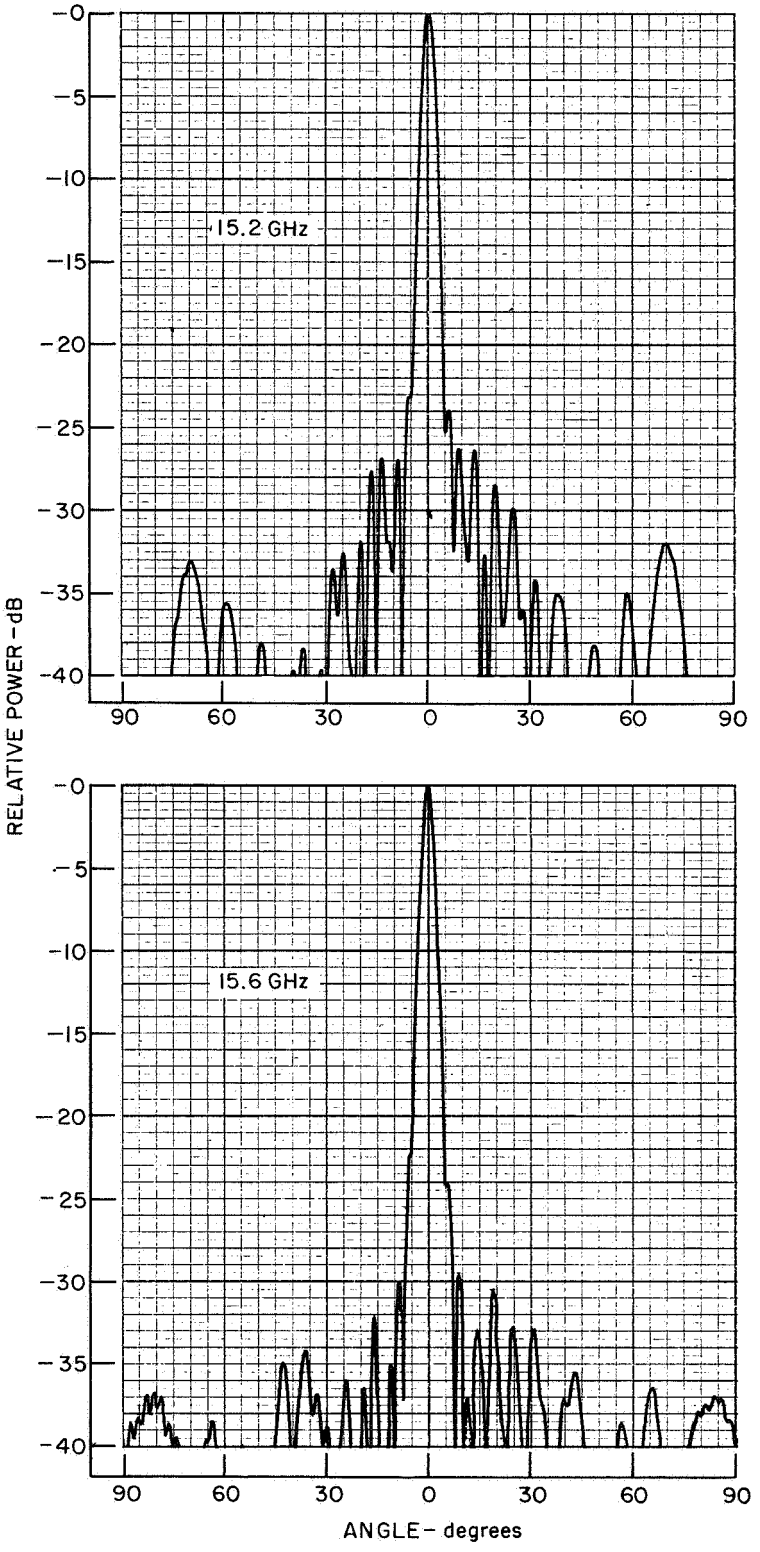

Figure 18. E-Plane Multi-Mode Horn Lens Patterns (Sheet 1 of 3)

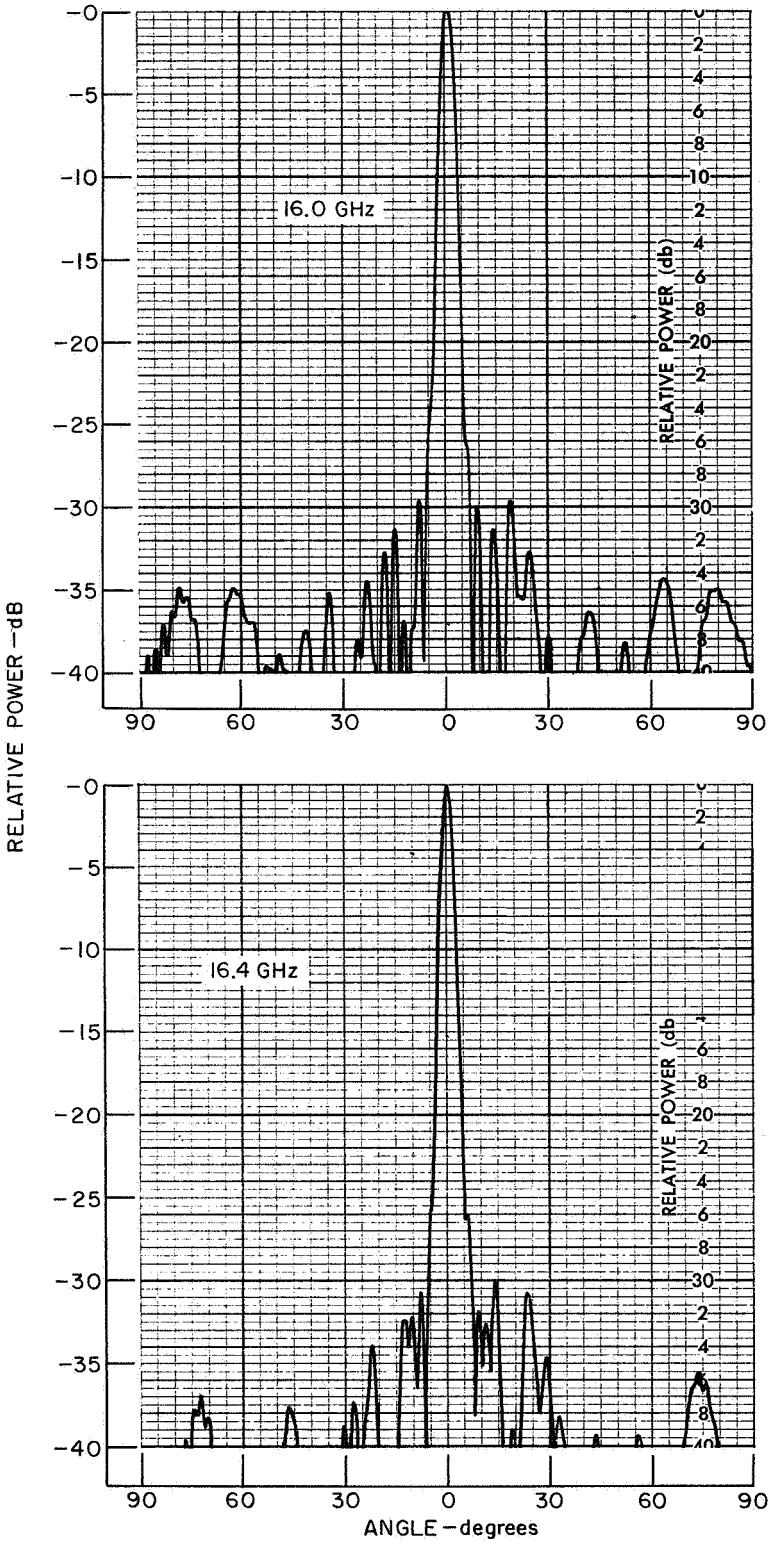

Figure 18. E-Plane Multi-Mode Horn Lens Patterns (Sheet 2 of 3)

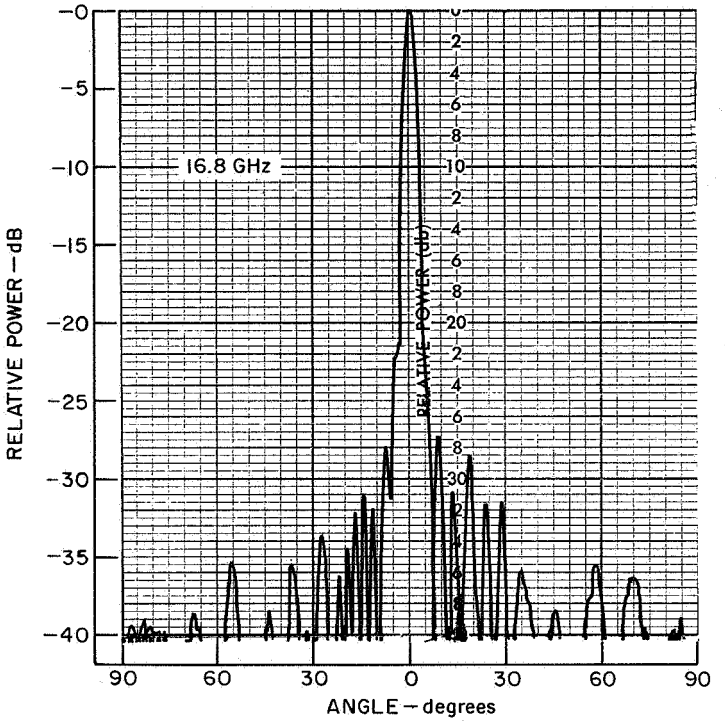

Figure 18. E-Plane Multi-Mode Horn Lens Patterns (Sheet 3 of 3)

An existing line source test fixture was modified to permit a sliding waveguide probe to sample the phase and amplitude output of individual elements of the power combiner. A plot of the output phase-amplitude characteristic of the combiner at 16.0 GHz is shown in Figure 20. The phase correction required per element for phase uniformity can be determined from this data.

A compensating adjustable phase shifter element, employing narrow-wall reactive screws in waveguide, was investigated to provide a phase adjustment capability on a per element basis in the combiner. This technique is easily implemented in the power combiner since the narrow waveguide walls of the divider section are readily accessable. A five-section phase shifter, shown conceptually in Figure 21, was evaluated to determined phase shift as a function of screw insertion. Spacing between screws is $\lambda g/4$ at the design frequency of 16.0 GHz. Phase shift and VSWR as a function of insertion turns are plotted in Figure 22. It is seen that inductive phase shift is available for limited screw insertion with very low VSWR. Beyond a point the phase shift reverses sign, the reactive elements become capacitive, and VSWR increases.

The prototype combiner was modified to accommodate the narrow-wall screw type phase shifter elements in each of its fifty ports. Phase correction was provided on a per element basis and the combiner patterns shown in Figure 23 were obtained.

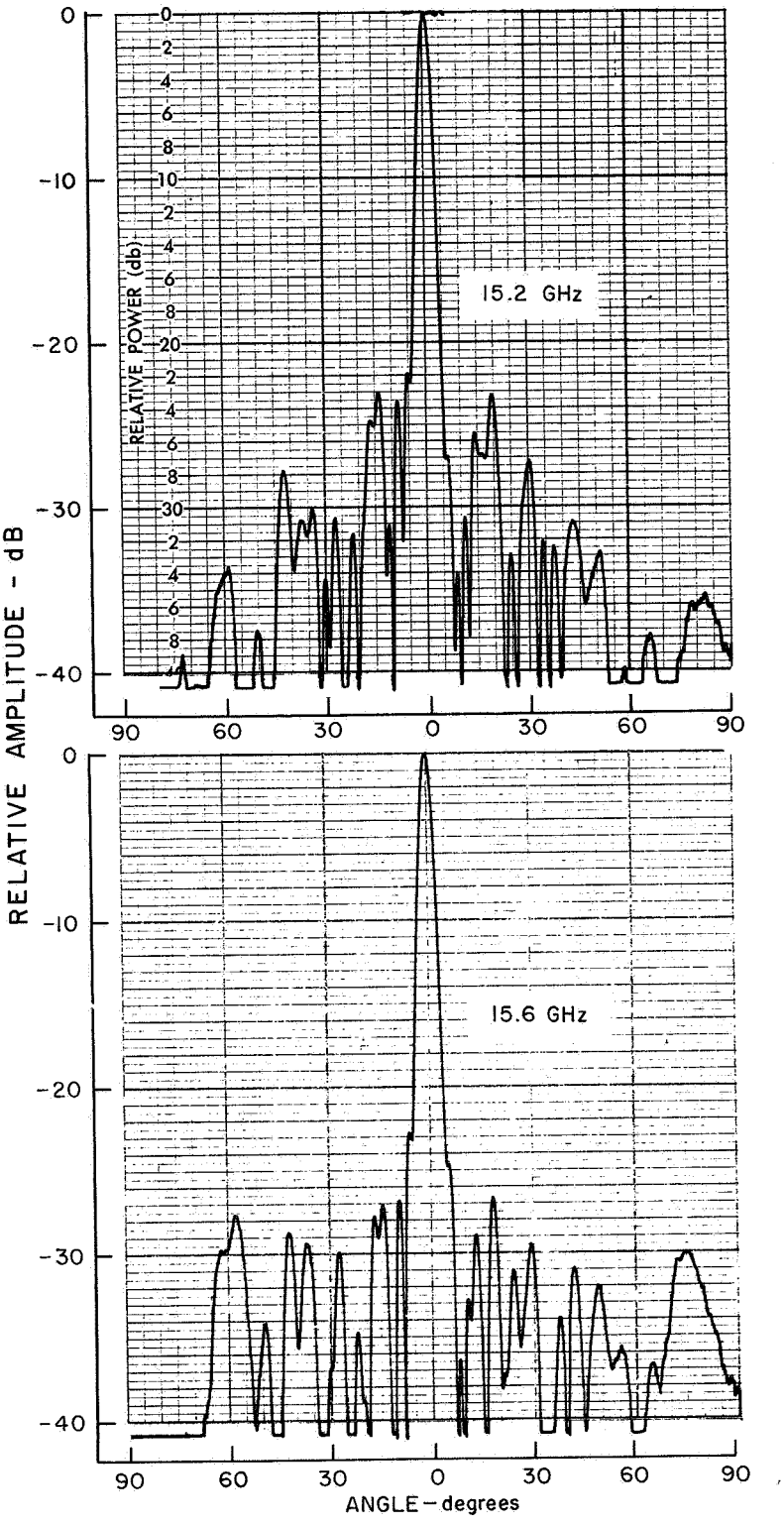

Figure 19. E-Plane 50-Way Power Combiner Patterns (Sheet 1 of 3)

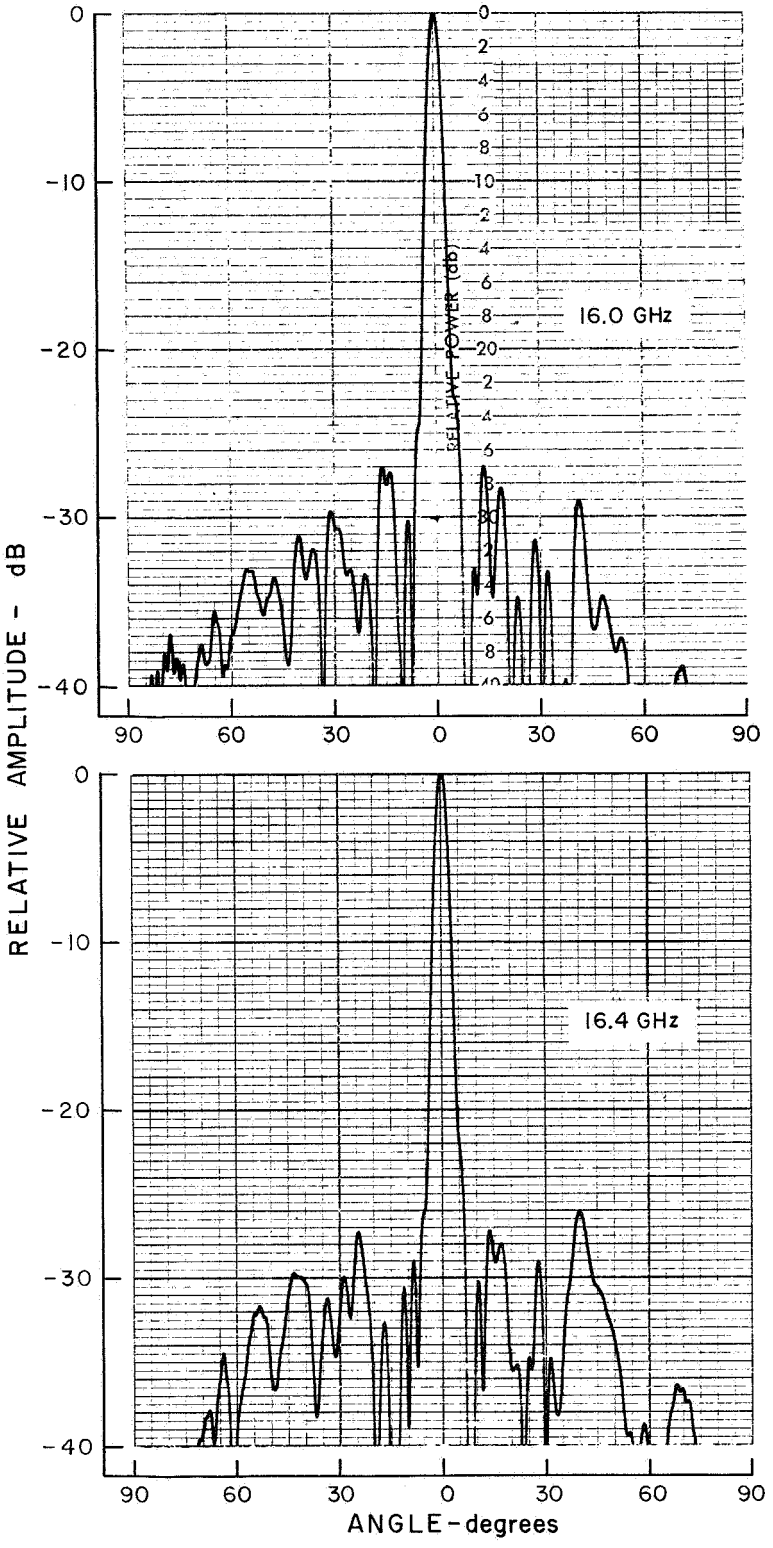

Figure 19. E-Plane 50-Way Power Combiner Patterns (Sheet 2 of 3)

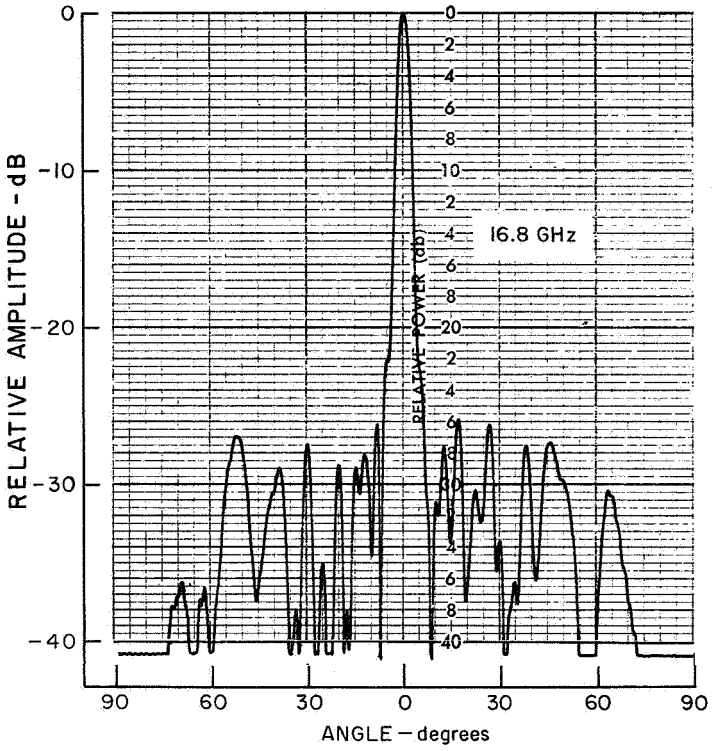

Figure 19. E-Plane 50-Way Power Combiner Patterns (Sheet 3 of 3)

The overall pattern improvement is observed by comparing the patterns of Figure 23 with those of Figure 19 noting the reduction of the average side lobe level, which is most apparent at mid-band.

The input VSWR of the uncorrected power combiner with all 50 ports terminated in matched loads was determined as a function of frequency. This data is shown in Figure 24. The VSWR plot of Figure 24 includes the effects of impedance mismatch due to both the mode generating step and lens-divider combinations. The effect of the mismatch of the mode generating step was removed by isolating its impedance characteristic and vectorially subtracting it from the impedance characteristic of the full combiner. The lens-divider VSWR obtained in this way is plotted vs. frequency in Figure 25. It is evident that a good impedance match has been obtained for the lens-divider section of the combiner over the 10% design frequency band. Addition of the phase correction screws to the divider has essentially no effect on the above impedance characteristics.

Radiation patterns of the power combiner-array combination shown in Figure 26 were measured over the 15.2 to 16.8 GHz frequency band. H-plane pattern data is essentially independent of which set of ten adjacent combiner ports is utilized. A set of H-plane patterns utilizing the center elements of the combiner, with remaining elements terminated in matched loads, is shown in Figure 27. There is essentially no difference between the H-plane array patterns and the individual element patterns

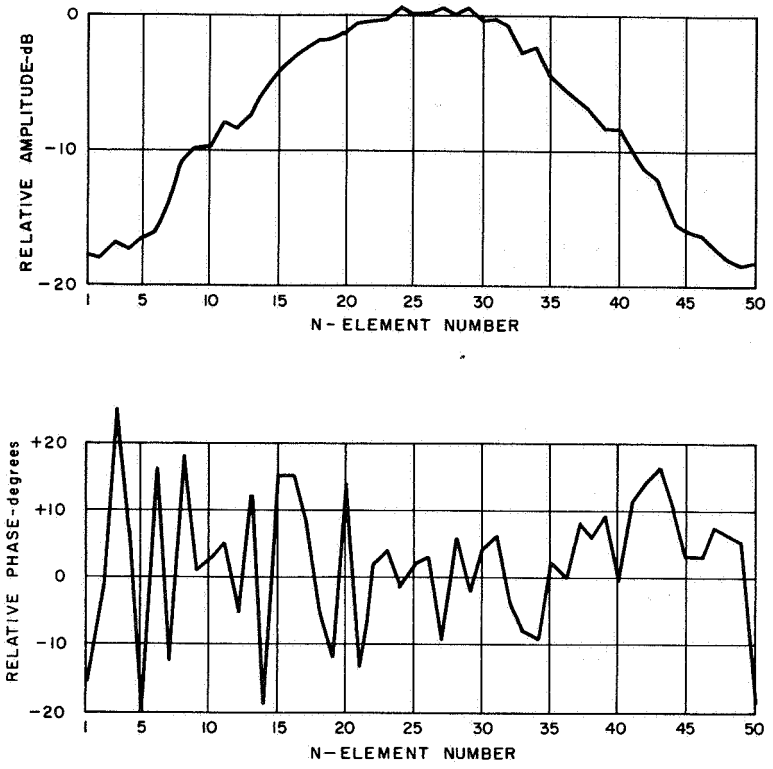

Figure 20. Uncorrected Amplitude and Phase Characteristics of the 50-Way Power Combiner at 16.0 GHz.

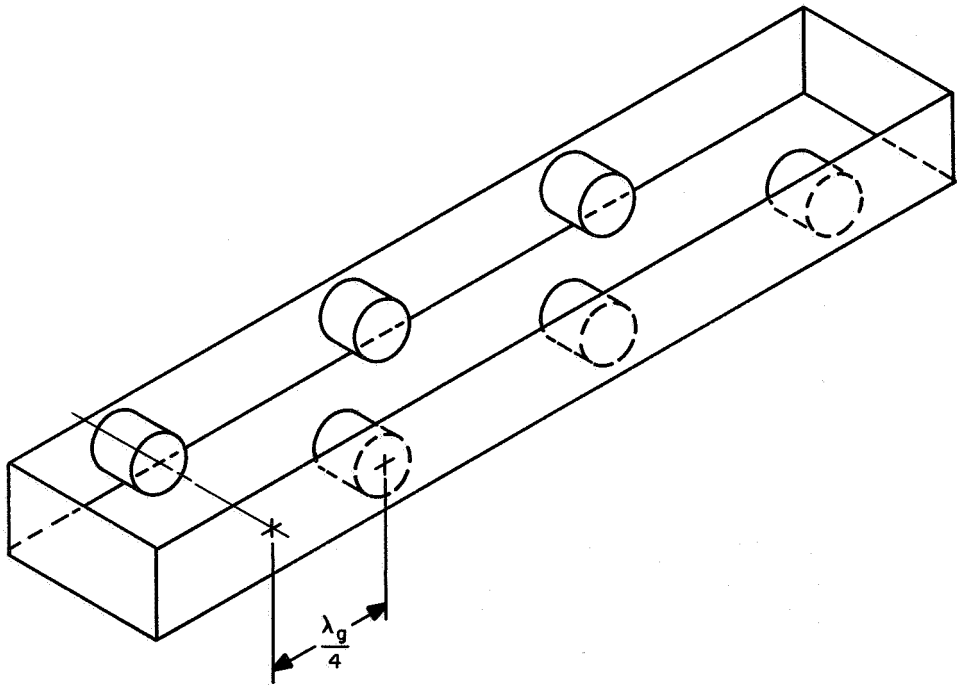

Figure 21. Five-Section Phase Shifter

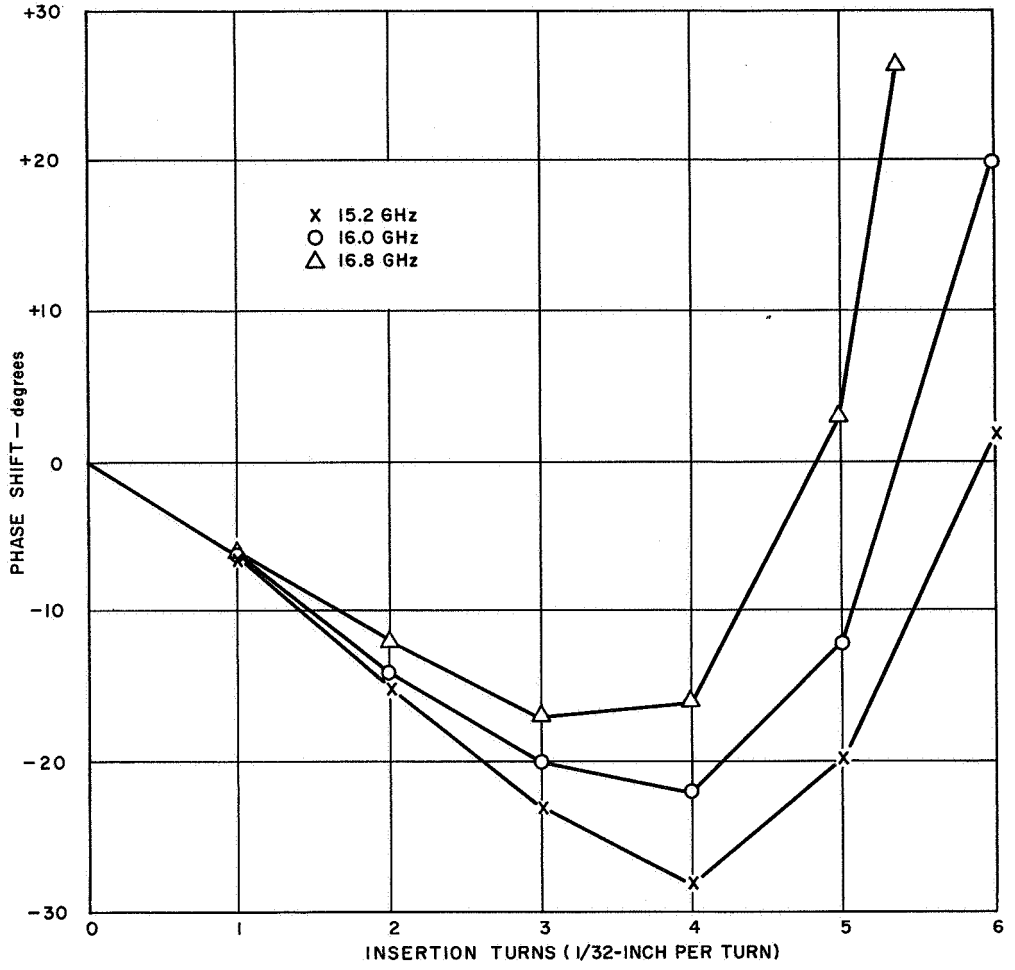

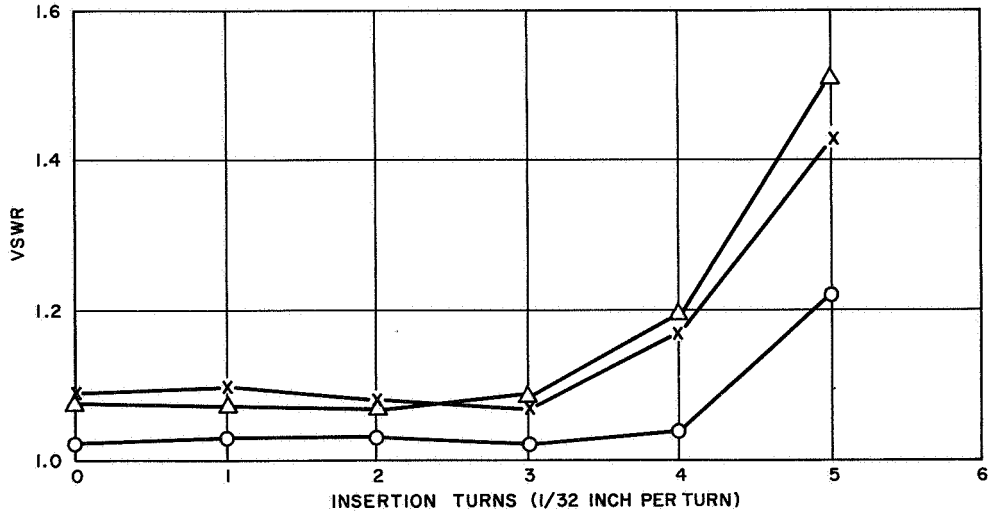

Figure 22. Phase Shift and VSWR as a Function of Screw Turns for 5-Section Phase Shifter

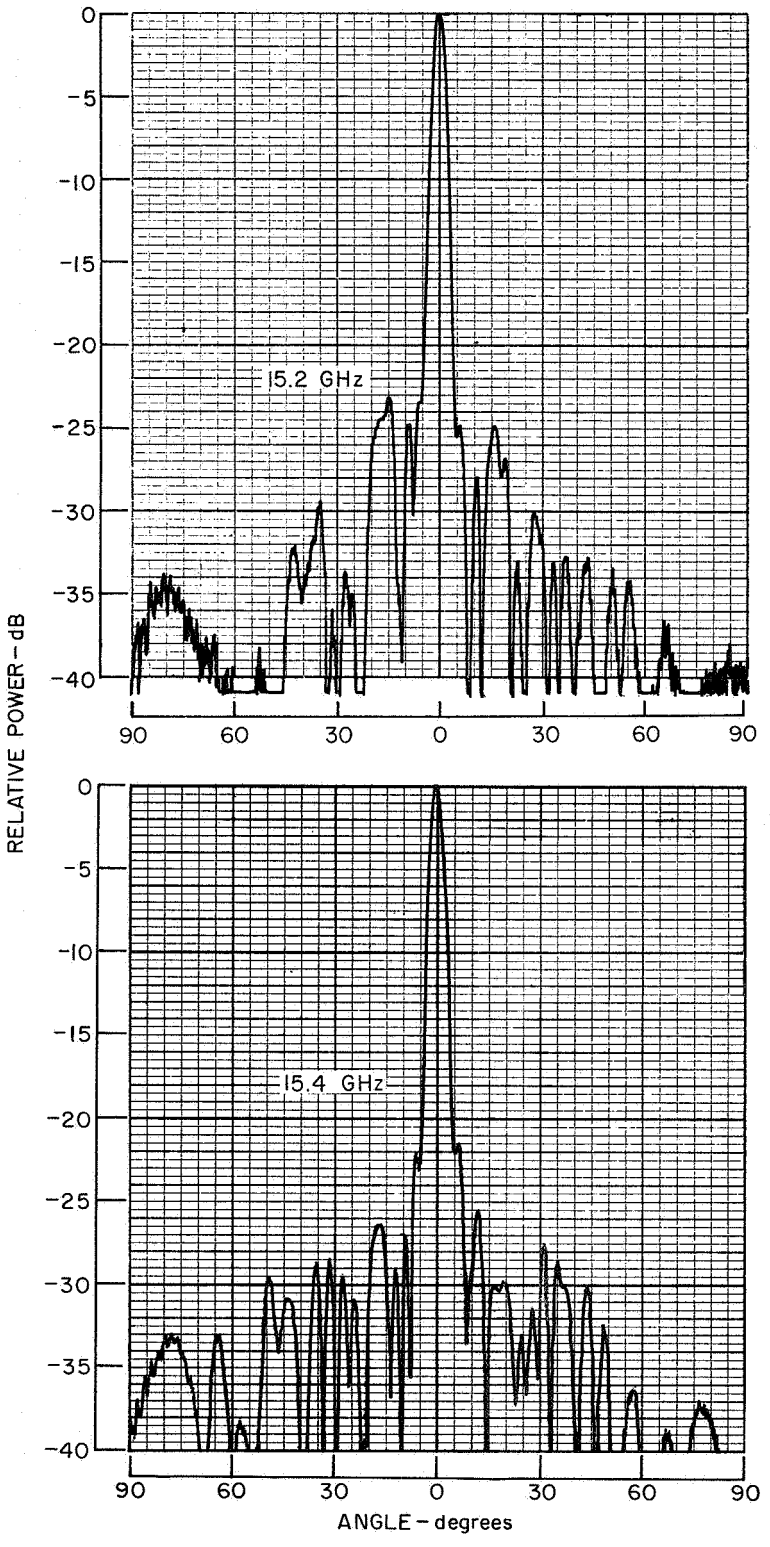

Figure 23. Phase-Corrected E-Plane 50-Way Power Combiner Patterns (Sheet 1 of 5)

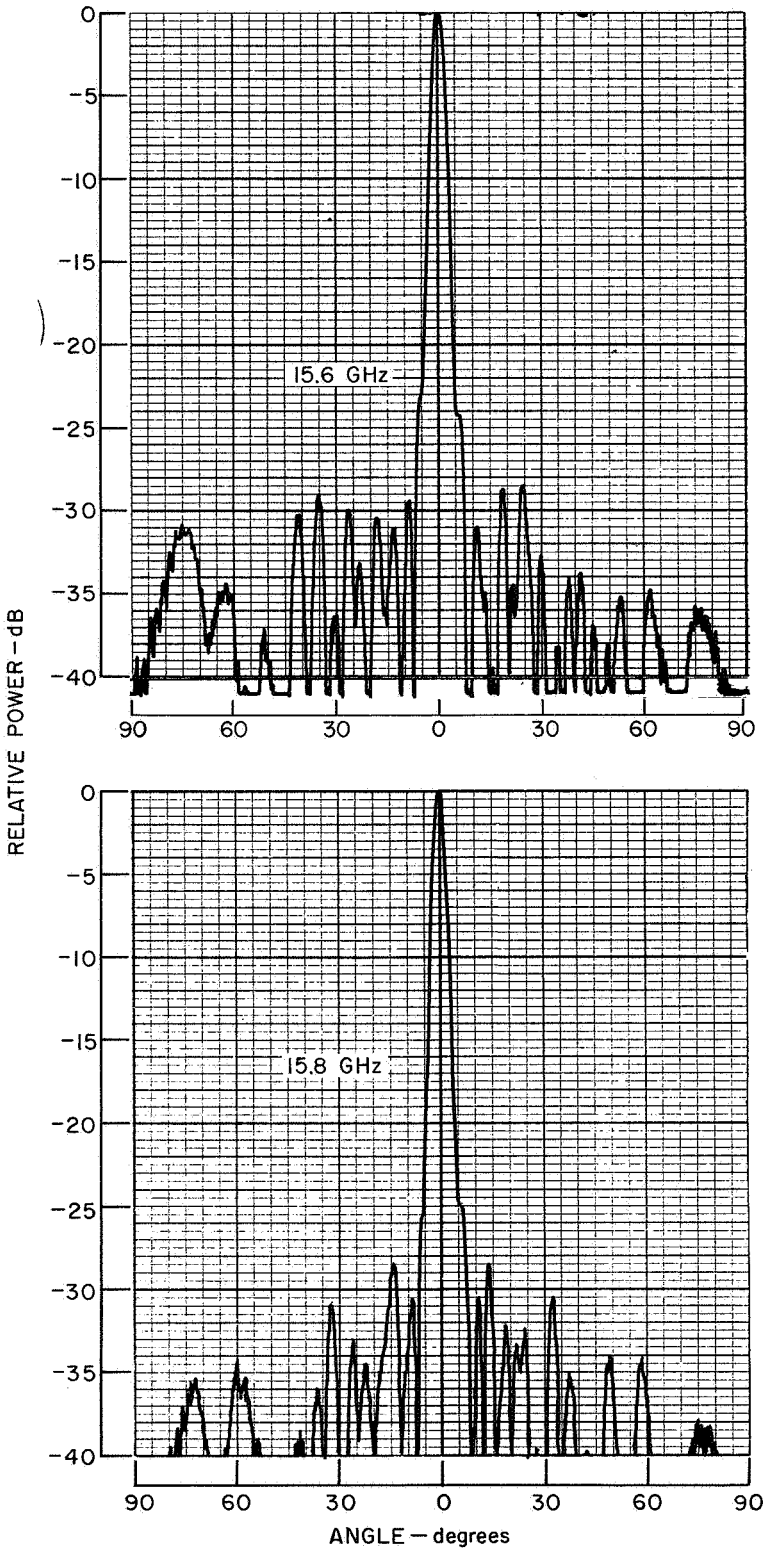

Figure 23. Phase-Corrected E-Plane 50-Way Power Combiner Patterns (Sheet 2 of 5)

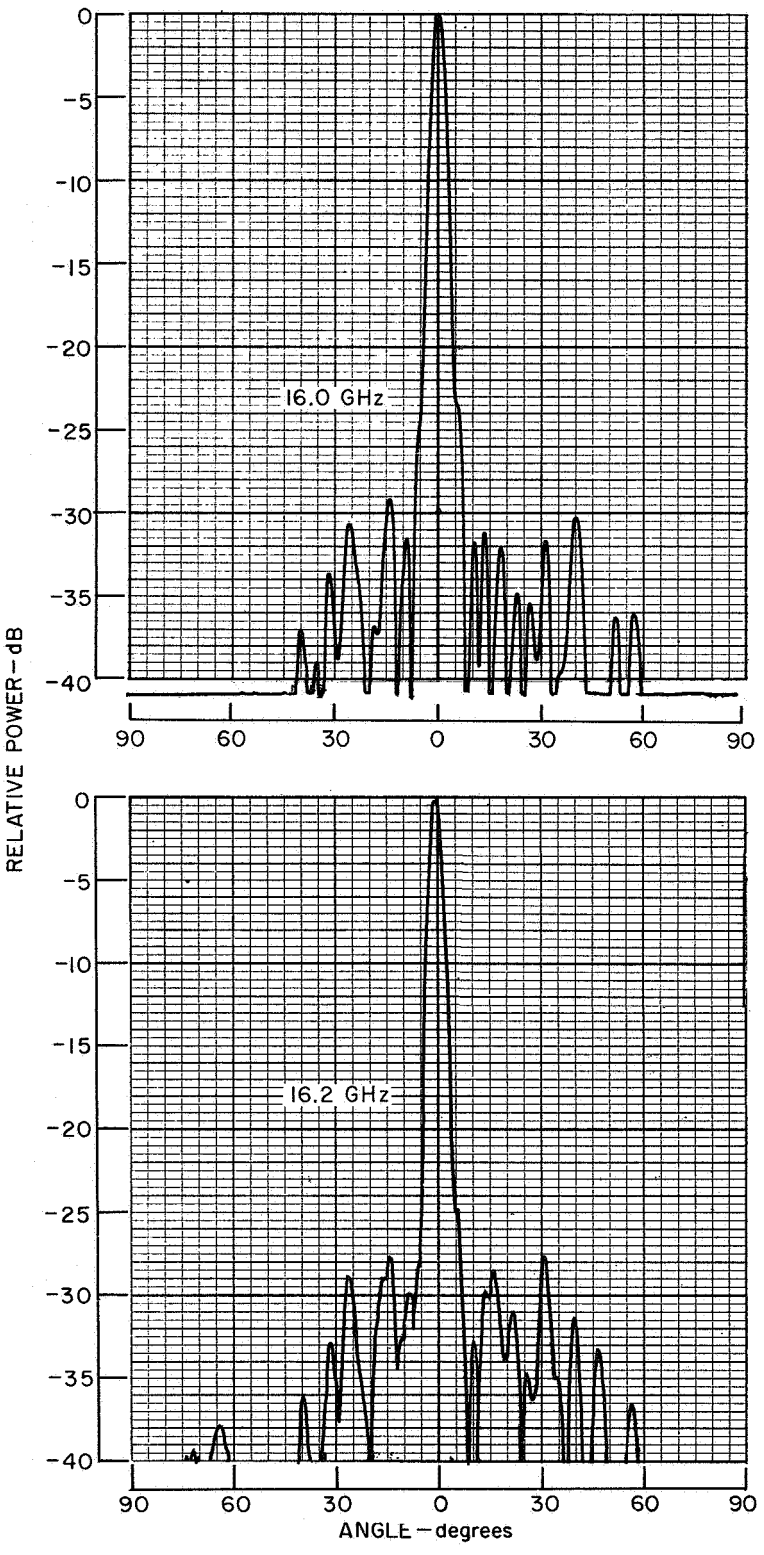

Figure 23. Phase-Corrected E-Plane 50-Way Power Combiner Patterns (Sheet 3 of 5)

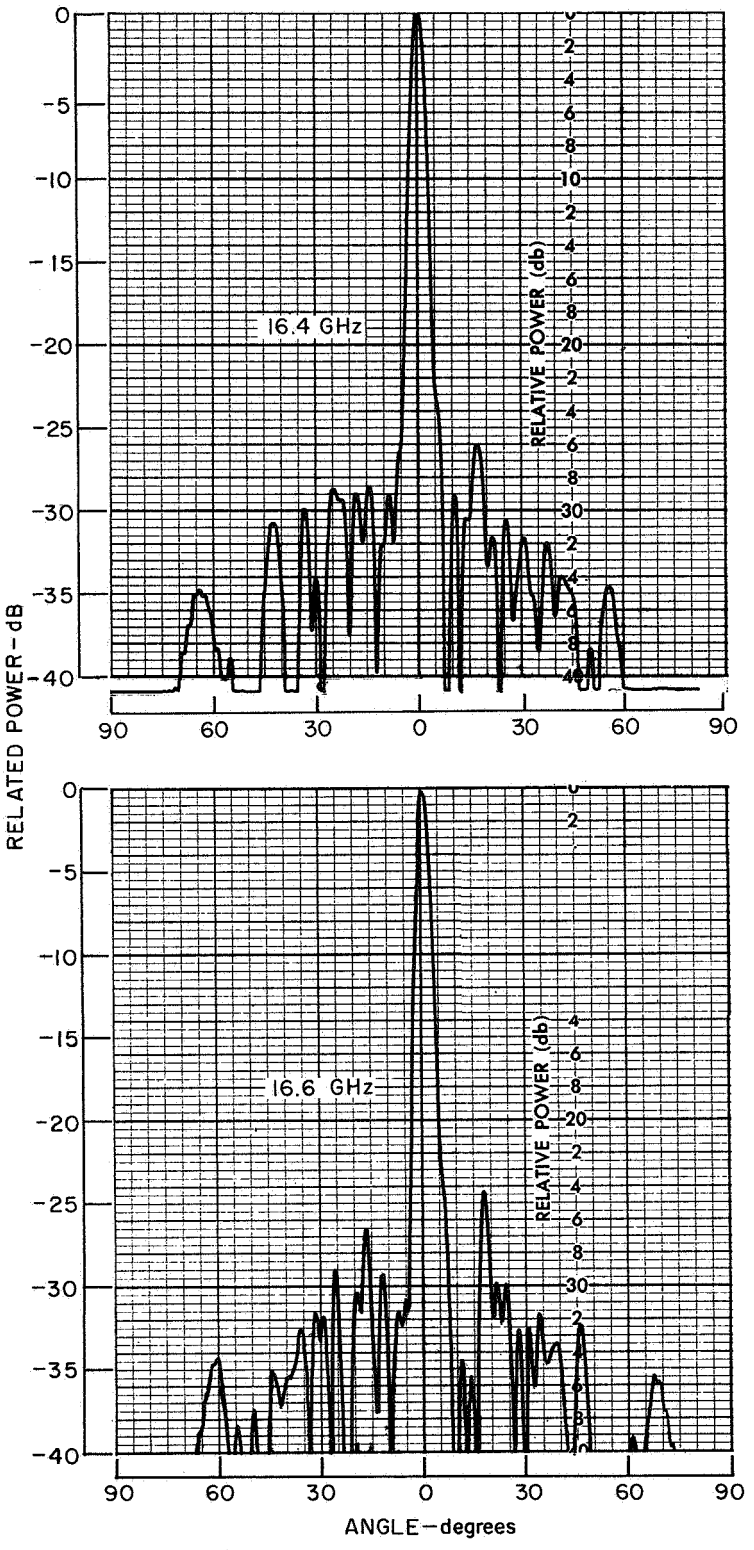

Figure 23. Phase-Corrected E-Plane 50-Way Power Combiner Patterns (Sheet 4 of 5)

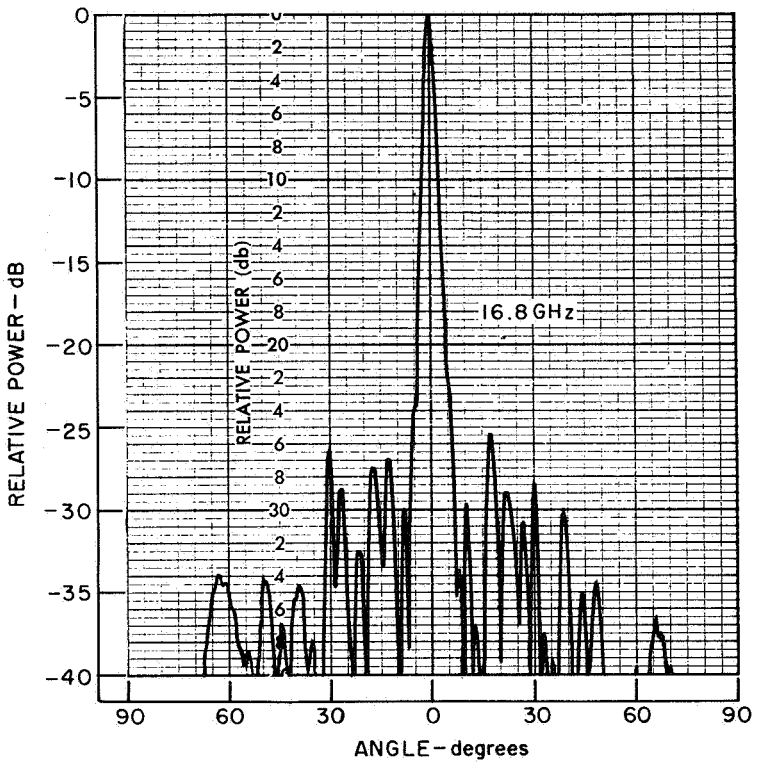

Figure 23. Phase-Corrected E-Plane 50-Way Power Combiner Patterns (Sheet 5 of 5)

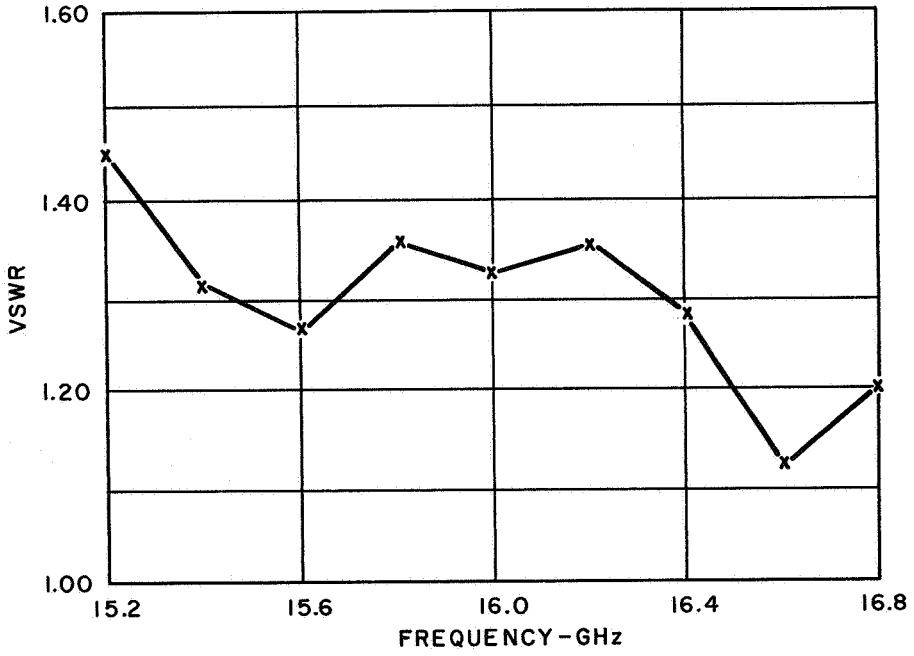

Figure 24. Power Combiner VSWR vs Frequency With All Ports Terminated in Matched Loads

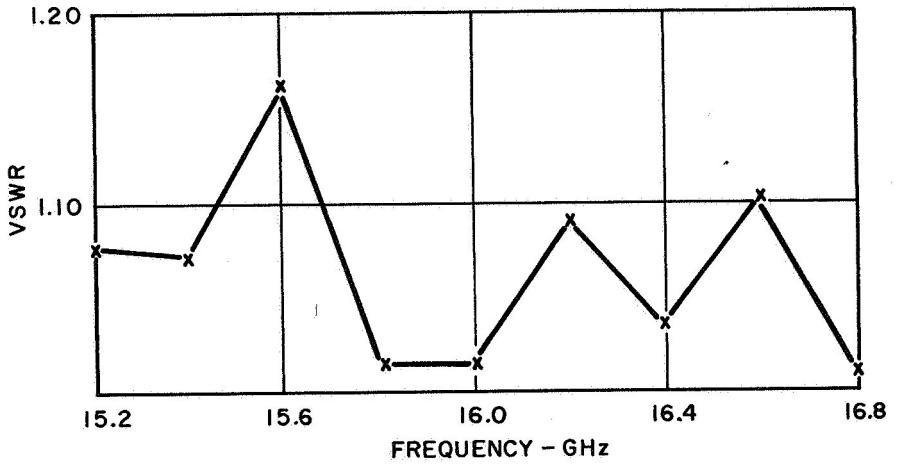

Figure 25. Lens-Divider Section of Power Combiner VSWR vs Frequency

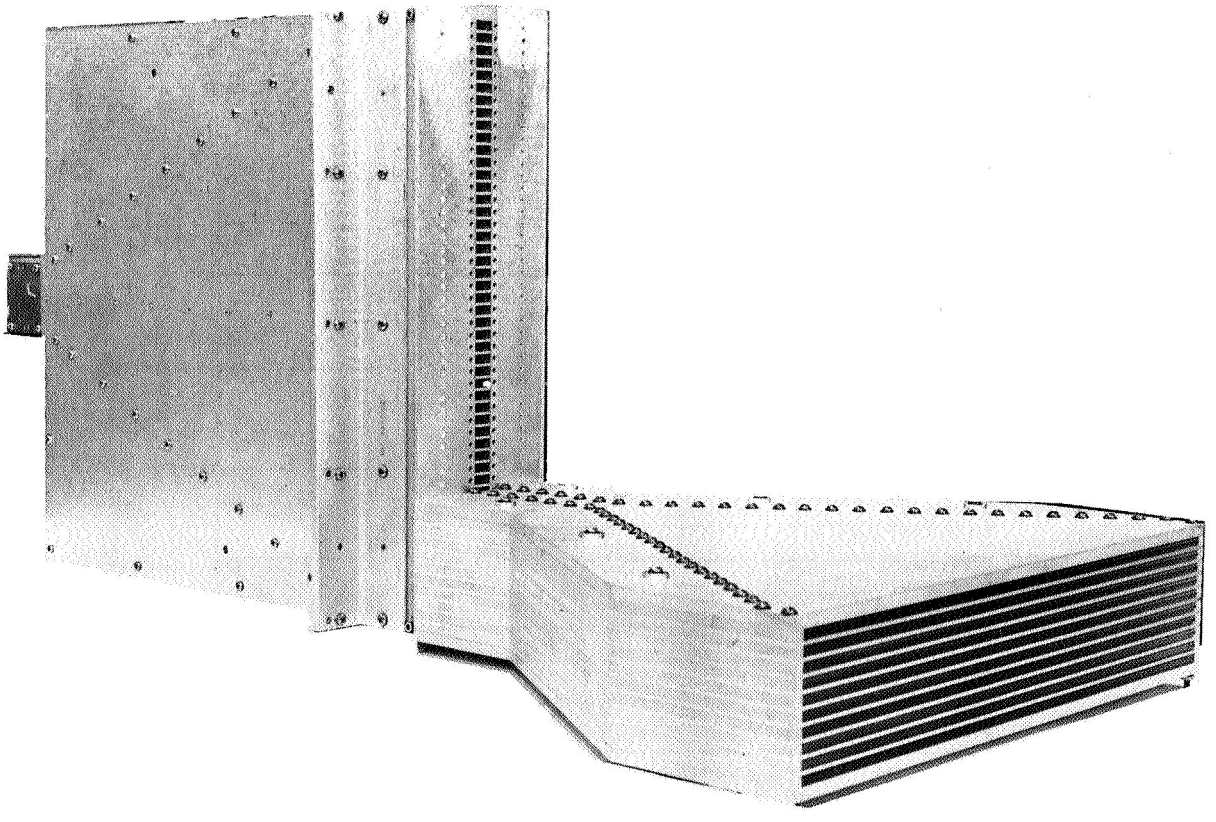

Figure 26. Ten-Element Array With 50-Way Power Combiner

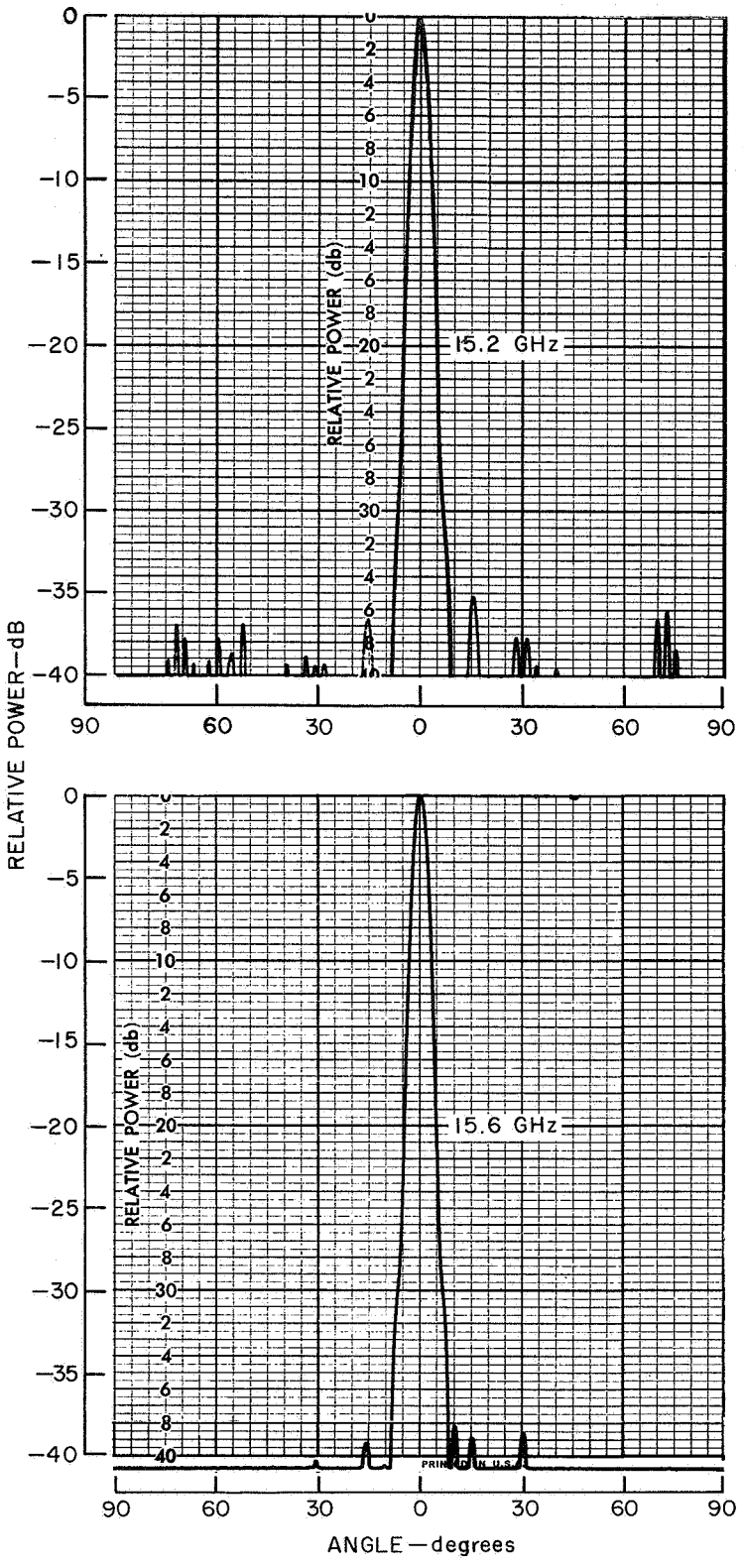

Figure 27. H-Plane Patterns for Power-Combiner/Array Configuration (Sheet 1 of 3)

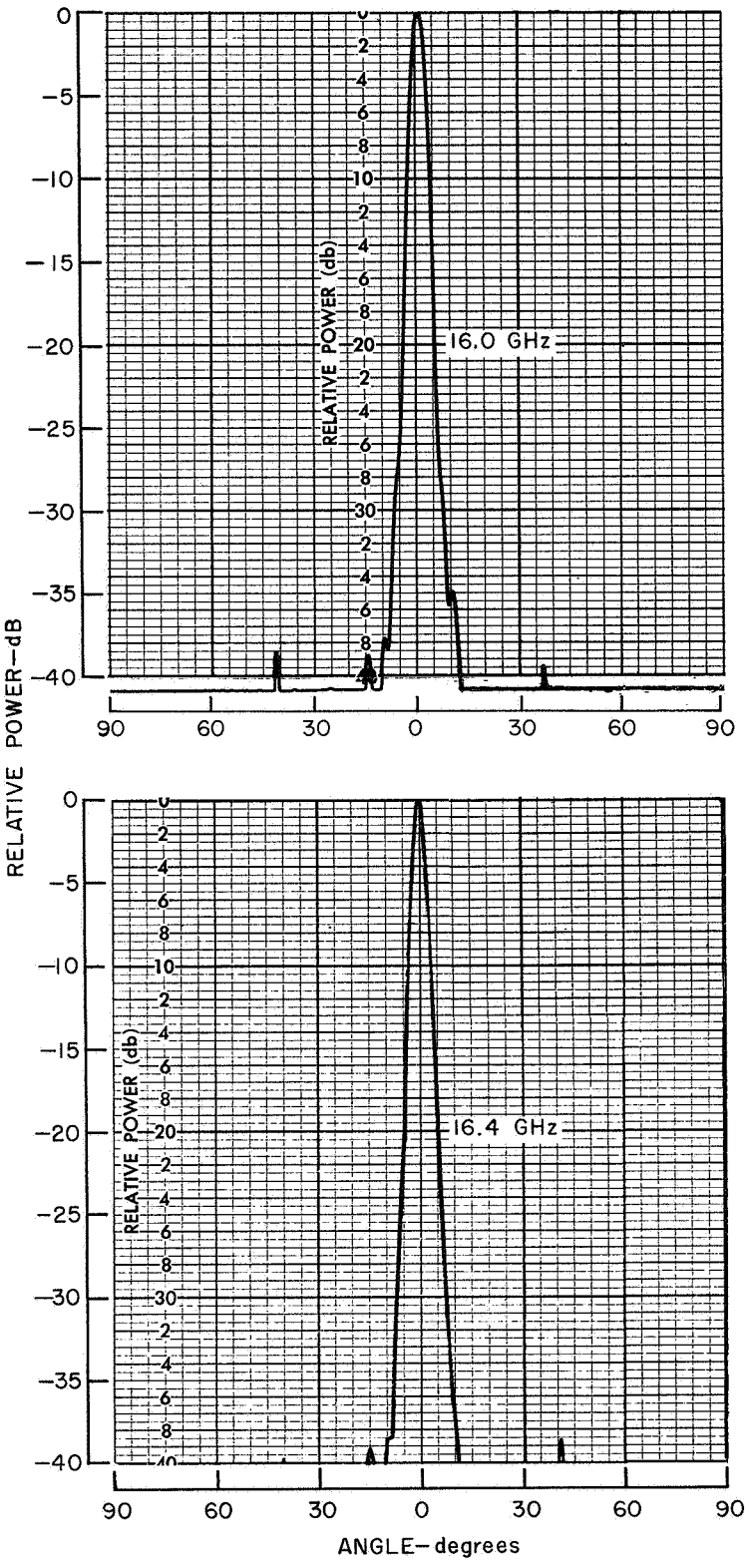

Figure 27. H-Plane Patterns for Power-Combiner/Array Configuration (Sheet 2 of 3)

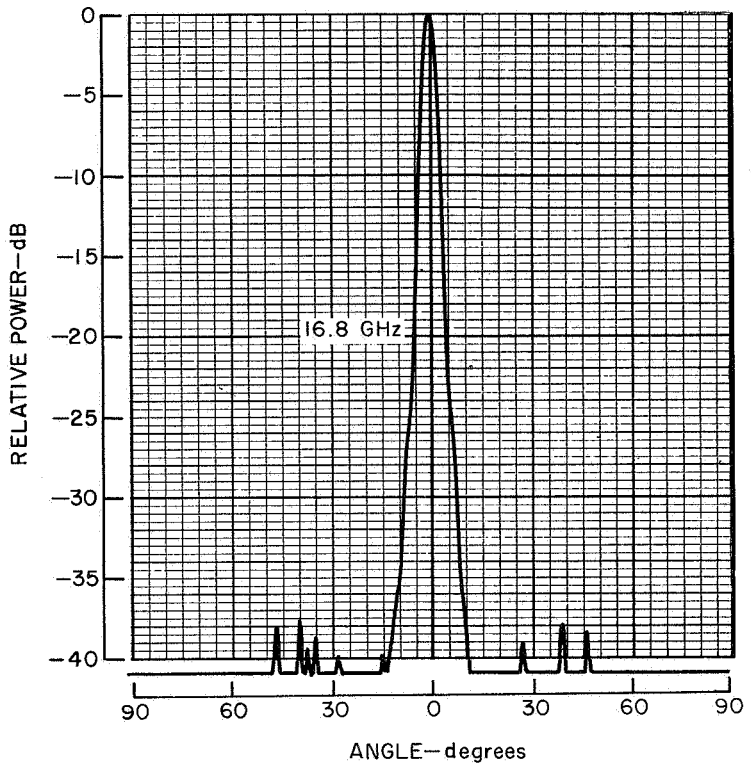

Figure 27. H-Plane Patterns for Power-Combiner/Array Configuration (Sheet 3 of 3)

of Figure 8. Some E-plane patterns were obtained but did not provide useful data due to the limited use of the full combiner output.

ARRAY PERFORMANCE

Broadside performance of a full array consisting of fifty H-plane sectoral horn-lens line source elements combined through a 50-way multimode combiner can be determined from measurements on the individual components.

Beam efficiency, which is of paramount importance, can be determined from measured patterns of the power combiner and line source elements.

The broadside beam efficiency, η_B, associated with an axially-symmetric antenna power pattern, $P(\theta, \phi)$, is given by equation 2.

$$\eta_B = \frac{\int_{\theta=o}^{\theta_N} \int_{\phi=o}^{\pi} P(\theta,\phi)\ \sin\theta\ d\theta d\phi}{\int_{\theta=o}^{\pi} \int_{\phi=o}^{\pi} P(\theta,\phi)\ \sin\theta\ d\theta d\phi} \tag{2}$$

where θ and ϕ are prime angles in the spherical coordinate system shown in Figure 28, and θ_N is the angle to the first pattern zero measured from the pattern axis.

Since $P(\theta, \phi)$ is not analytically specified, η_B may be determined from the following approximate expression,

$$\eta_B \doteq \frac{\sum_{\phi} \int_{o}^{\theta_N} P(\theta)\ \sin\theta\ d\theta}{\sum_{\phi} \int_{o}^{T} P(\theta)\ \sin\theta\ d\theta} \tag{3}$$

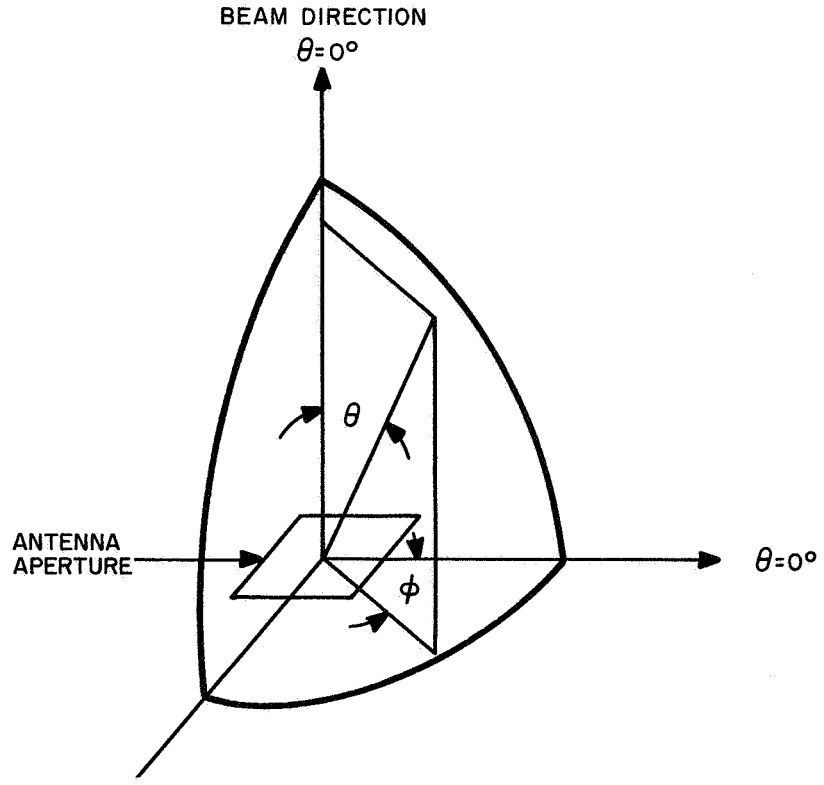

Figure 28. Spherical Coordinate System

where the function $P(\theta) \sin \theta$ can be determined from measured single-plane pattern data and integrated with a planimeter.

The approximate expression for beam efficiency will give reasonably accurate results if the principal and diagonal planes of the array are considered so that equation (3) becomes

$$\eta_B \doteq \frac{A_E + A_H + 2A_{45°}}{A_{ET} + A_{HT} + 2A_{45°T}} \tag{4}$$

$$\text{where } A_i = \int_0^{\theta_N} P_i(\theta) \sin \theta \, d\theta$$

$$A_{it} = \int_0^{\pi} P_i(\theta) \sin \theta \, d\theta$$

and the E-, H-, and 45° subscripts denote the E-, H-, and 45°-pattern planes respectively.

The broadside E- and H-plane patterns of the full array will essentially equal the power combiner and line source element patterns, respectively. The 45°-plane pattern for a highly directive square array, $P_{45°}(\theta)$, can be accurately determined from the following approximation.

$$P_{45°}(\theta) \doteq P_E\left(\frac{\theta}{\sqrt{2}}\right) P_H\left(\frac{\theta}{\sqrt{2}}\right) \tag{5}$$

and is used to obtain the 45°-plane terms in equation (4).

Beam efficiency for a 17.6-inch square array, defined by the prototype H-plane elements and fifty-way combiner, was calculated over a 15.2 to 16.8 GHz frequency band using the pattern data of Figures 8 and 23.

Projected array beam efficiency vs. frequency is plotted in Figure 29. From this data, it is seen that the maximum computed beam efficiency exceeds 0.96 at the design frequency 16.0 GHz. Beam efficiency deteriorates to 0.90 at 15.2 GHz and 0.93 at 16.8 GHz. Beam efficiency exceeds 0.90 over the full 10% frequency band and 0.93 over the 7.4% band from 15.6 to 16.8 GHz.

PHASE SHIFTER STUDY

A study has been made to determine the configuration of a ferrite phase shifter for use from 15.2 to 16.8 GHz.

Theoretical calculations have been made by solving Maxwell's equations in the waveguide whose cross section is shown in Figure 30. Regions I, II, IV comprise a representation of a rectangular ferrite toroid with a slot loaded with a dielectric of relative permittivity Ke. The boundary conditions lead to the transcendental equations for the propagation constant, β.

$$\tan k_3 a = \frac{k_3 \left[\frac{k_1}{\rho^2} - \frac{j\beta}{\rho\theta} \cot(k_1\delta_2) - \frac{k_2}{\rho} \cot(k_2\delta_1) \cot(k_1\delta_2) \right]}{\left(\frac{\beta^2}{\theta^2} - k_2^2 \right) \cot(k_1\delta_2) - \frac{k_1 k_2}{\rho} \cot(k_2\delta_1) + \frac{j\beta k_1}{\rho\theta}}$$

where

$$k_1 = \sqrt{Ke\,\omega^2 \mu_o \epsilon_o - \beta^2} \; ; \; k_2 = \sqrt{\frac{K_m}{\rho} \mu_o \epsilon_o - \beta^2} ; \; k_3 = \sqrt{\omega^2 \mu_o \epsilon_o - \beta^2}$$

$$\rho = \frac{1}{1+\chi_{xy}^2} \; ; \; \theta = \frac{1}{\chi_{xy}} \; ; \; \chi_{xy} = \frac{j\omega\gamma(4\pi M_r)}{\omega^2}$$

γ = 2.8 MHz/oe.

This equation applies in the case where the ferrite is in its remanent state with magnetization $4\pi M_r$. By solving for β while changing the sign of $4\pi M_r$, one obtains two solutions whose difference is the differential phase shift. The equation is solved on a digital computer using an iterative approach. In this way, many different combinations of dimensions and materials can be tested.

Since the actual toroid has a shape as shown in Figure 31, the "bridges" at top and bottom must be accounted for, as they degrade the phase shift with respect to the theoretical model. This is done by multiplying the result by an emperical factor $1 - \frac{xt}{h}$

where $1 < x < 2$

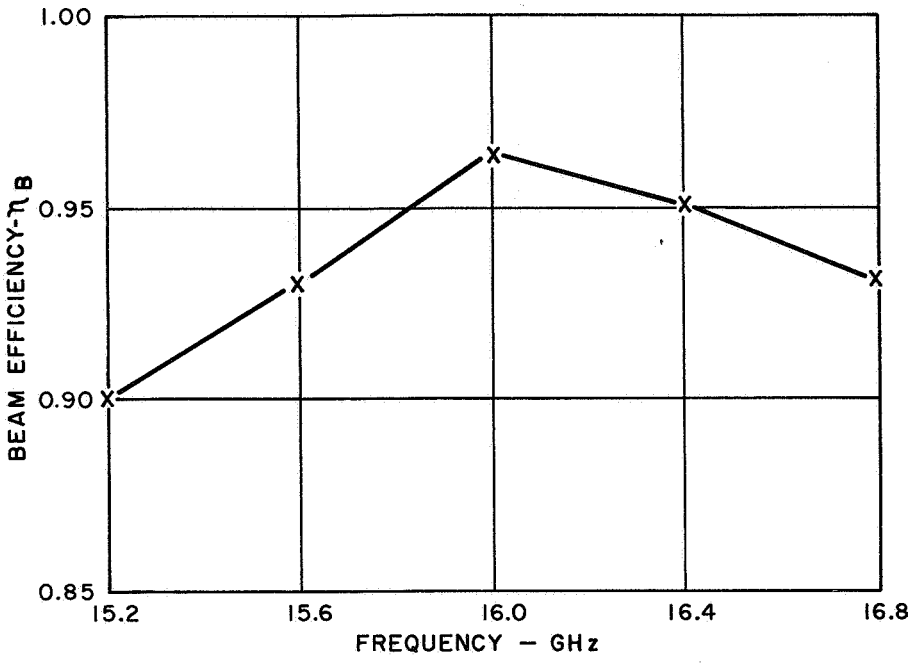

Figure 29. Projected Array Beam Efficiency

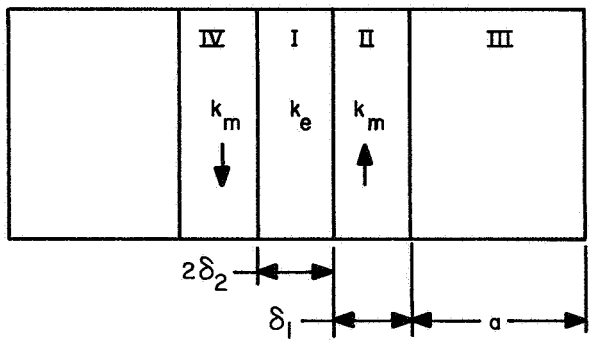

Figure 30. Ferrite-Loaded Waveguide Cross Section

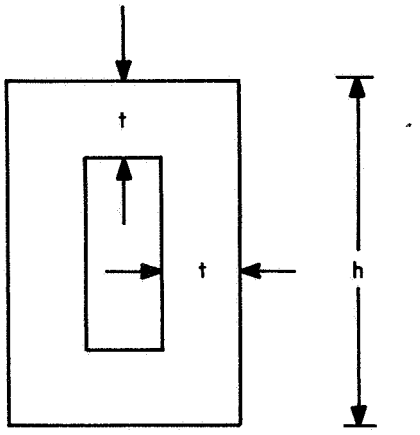

Figure 31. Toroid Shape

Solutions for the 0.622 by 0.259-inch waveguide using a commercially available ferrite (Trans-Tech Inc. TT1-390) give a toroid width of 0.100-in. with a 0.025-in slot loaded with K = 16. Theoretical phase shift is 162°/inch.

Two step transformers are used to match the ferrite loaded section to the empty waveguide. These are fabricated from K = 6 Stycast (Emerson and Cuming Inc.) to dimensions determined by computer solution of a waveguide loaded with a single dielectric slab.

The phase shifter can be driven in two ways. As a multiple bit phase shifter, the ferrite is divided into different length sections each of which can be magnetized separately to the maximum remanent state, yielding digital steps of phase shift.

Magnetization is accomplished by passing a current through a one-turn magnetizing winding for each section which enters the side wall of the guide and threads through the toroid. Dielectric separators maintain waveguide loading and provide magnetic isolation between the sections.

The flux drive phase shifter uses a single section of ferrite of sufficient length to give the maximum phase shift desired. Smaller phase shifts are accomplished by partially magnetizing, rather than saturating the ferrite. The flux drive scheme requires,

at most, two wires to the phase shifter and one driver. It is able to compensate for changes in the magnetic properties of the ferrite at the expense of some complexity of the circuit. It is inherently an analog phase shifter although it is usually used as a digital device by feeding digital phase commands into a digital-to-analog converter. The multiple bit phase shifter requires one wire and one driver to each bit, but the drivers are much simpler than those of the flux driver, since they always saturate the ferrite and do not have to control the amount of flux fed to the phaser.

Phase shift for a multiple bit device is nearly proportional to magnetization so material tolerances and temperature variations of magnetic properties most directly affect phase shift. In the flux drive phase shifter, errors are caused by circuit non-linearities and also by changes in material parameters in the partially magnetized state which have not been explained to date. The choice between multiple bit and flux drive will be affected by considerations associated with the radiometer and space-craft systems.

The estimated weight of a 5-bit ferrite phase shifter element for the Ku-band array waveguide size is 1.12×10^{-2} pounds. The weight of 50 such elements, as required for the full array, is estimated to be 0.56 pounds. Estimated loss for the phase shifter is 0.5 dB.

Phase tolerances can be maintained extremely small in a relatively fixed temperature environment. Phase shifters can be individually trimmed for greater accuracy.

CONCLUSIONS

The H-plane sectoral horn-lens line source provides radiation patterns with extremely low sidelobes over a very wide frequency band leading to high beam efficiency in an array configuration.

The ten-element array verified the desirable radiation characteristics of the H-plane line source; it also revealed the line source pattern, impedance, and gain characteristics to be relatively independent of element location in the array. Inter-element coupling was found to agree very closely with that predicted for a similar array of parallel plate waveguides.

The multi-mode 50-way power combiner patterns were found to agree very closely with those of its multi-mode horn alone. Low sidelobe characteristics were observed at the design frequency with some expected deterioration at the edges of a ten per cent frequency band.

Projected array performance, using measured patterns of both the ten-element array and 50-way power combiner, indicates that beam efficiency exceeds 90 per cent over a 10 per cent frequency band, 93 per cent over a 7.4 per cent frequency band and 96 per cent at center frequency.

Phase shifter studies revealed no significant difficulties in design or development of a Ku-band ferrite phase shifter for this array application.

REFERENCES

1. C. E. Profera Jr.: Phased Arrays for Meteorological Satellite. Interim Report No. 1, NAS-12-149, June 1967.

2. E. M. T. Jones, T. Morita and S. B. Cohn: Measured Performance of Matched Dielectric Lenses. IRE Transactions on Antennas and Propagation, January 1956.

3. T. Morita and S. B. Cohn: Microwave Lens Matching by Simulated Quarter-Wave Transformers. IRE Transactions on Antennas and Propagation, January 1956.

4. S. Lee: Radiation from an Infinite Array of Parallel-Plate Waveguides. IEEE Transactions on Antennas and Propagation, Sept. 1967.

New Technology Appendix

MULTIMODE N-WAY POWER COMBINER

This item is described on pages 17, 25, 29, and 32 and in the figures as referenced on those pages.